THE JOURNAL OF PHYSICAL CHEMISTRY B

Article

Cite This: J. Phys. Chem. B 2018, 122, 9665−9680

pubs.acs.org/JPCB

Hydrogen-Rich Cation Radicals of DNA Dinucleotides: Generation and Structure Elucidation by UV−Vis Action Spectroscopy

Yang Liu,[†] Joseph A. Korn,[†] Andy Dang, and František Tureček*

Department of Chemistry, Bagley Hall, University of Washington, P.O. Box 351700, Seattle, Washington 98195-1700, United States

Supporting Information

ABSTRACT: Hydrogen-rich DNA dinucleotide cation radicals $(dGG + 2H)^{+\bullet}$, $(dCG + 2H)^{+\bullet}$, and $(dGC + 2H)^{+\bullet}$ represent transient species comprising protonated and hydrogen atom adducted nucleobase rings that serve as models for proton and radical migrations in ionized DNA. These DNA cation radicals were generated in the gas phase by electron-transfer dissociation of dinucleotide dication−crown−ether complexes and characterized by UV−vis photodissociation action spectra, ab initio calculations of structures and relative energies, and time-dependent density functional theory calculations of UV−vis absorption spectra. Theoretical calculations indicate that $(dGG + 2H)^{+\bullet}$ cation radicals formed by electron transfer underwent an exothermic conformational collapse that was accompanied by guanine ring stacking and facile internucleobase hydrogen atom transfer, forming 3′-guanine C-8−H radicals. In contrast, exothermic hydrogen transfer from the 5′-cytosine radical onto the guanine ring in $(dCG + 2H)^{+\bullet}$ was kinetically hampered, resulting in the formation of a mixture of 5′-cytosine and 3′-guanine radicals. Conformational folding and nucleobase stacking were energetically unfavorable in $(dGC + 2H)^{+\bullet}$ that retained its structure of a 3′-cytosine radical, as formed by one-electron reduction of the dication. Hydrogen-rich guanine $(G + H)^{\bullet}$ and cytosine $(C + H)^{\bullet}$ radicals were calculated to have vastly different basicities in water, as illustrated by the respective pK_a values of 20.0 and 4.6, which is pertinent to their different abilities to undergo proton-transfer reactions in solution.

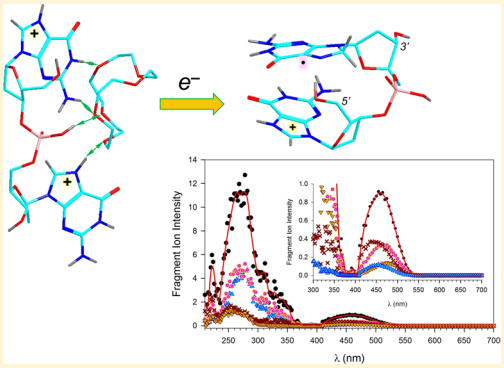

INTRODUCTION

DNA ionization by high-energy particles is a major cause of chemical changes leading to the complex process of DNA damage.[1] Ionization randomly creates an electron defect (a "hole") in a nucleobase that can propagate by charge transfer along the double strand to generate reactive intermediates undergoing further radical reactions.[2−7] Although the chemistry of hole generation and propagation dynamics has been studied for over two decades with ingenious model systems, the intrinsic electronic properties of the reactive cation radical intermediates have been elucidated only recently.[8−14] For example, Schuster and co-workers examined adenine−thymine-rich nucleic acid models that upon one-electron oxidation underwent reactions, indicating proton-coupled electron transfer between the ionized adenine and thymine nucleobases.[8] Proton transfer between ionized cytosine and guanine nucleobases in Watson−Crick pairs has been studied computationally[15−23] and by gas-phase experiments.[24]

In addition to standard studies of DNA ionization in solution, there have been several studies aimed at generating and characterizing nucleobase,[25−32] and nucleoside[24] radicals and cation radicals in the gas phase. By excluding interactions with solvent and counterions, gas-phase studies allow one to address the intrinsic electronic and chemical properties of the radical species of interest.[33] In addition, by using tandem mass spectrometry, one can achieve specific generation and isolation of cation radicals that can be further probed by UV−vis photodissociation action spectroscopy (UVPD) in the infrared and UV−visible regions of the spectrum. Recently, we have reported a novel type of DNA and chimeric RNA dinucleotide cation radicals that were studied in the gas phase.[34] These novel radical species were generated by ion−ion reactions of doubly protonated dinucleotides with molecular anions,[35] specifically fluoranthene anion radicals[36] (Scheme 1), whereby one-electron reduction in the gas phase was utilized as a versatile synthetic tool. We call these species hydrogen-rich DNA cation radicals because they contain two additional hydrogen atoms, one attached as the charging proton and the other introducing the unpaired electron into the DNA molecule. The term "hydrogen-rich" was coined previously for peptide cation radicals analogously generated by electron transfer to multiply protonated peptides and proteins.[37,38]

Hydrogen-rich DNA cation radicals having adenine nucleobases, such as $(dAA + 2H)^{+\bullet}$, have been found to exhibit interesting electronic properties and reactivity.[34] In particular, electron transfer to the dications caused major conformational changes associated with the stacking of the

Received: August 14, 2018
Revised: September 25, 2018
Published: September 30, 2018

DOI: 10.1021/acs.jpcb.8b07925
J. Phys. Chem. B 2018, 122, 9665−9680

Scheme 1. Formation of Hydrogen-Rich Dinucleotide Cation Radicals by One-Electron Reduction of Dications

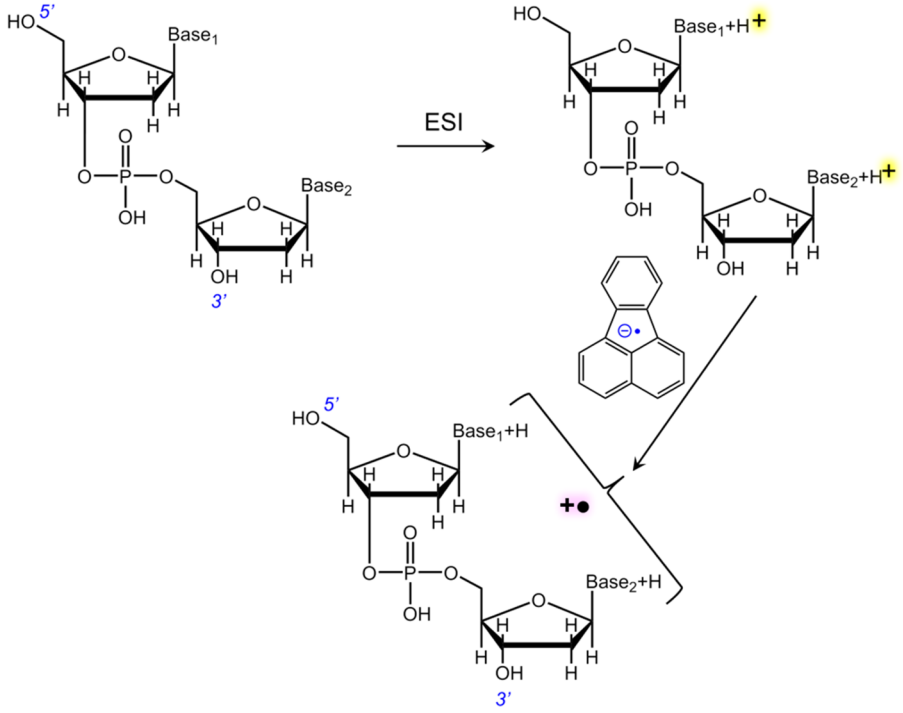

adenine cation and radical moieties that was followed by spontaneous interbase proton transfer.

Hydrogen-rich DNA dinucleotide radicals are related to reactive intermediates produced by the attachment of low-energy electrons to DNA nucleobases.[39] With purine nucleobases, fast electron attachment forms a transient anion radical, which is protonated by solvent on a microsecond time scale.[40] The resulting radical is a hydrogen-atom adduct to the nucleobase, which is analogous to the gas-phase species generated by electron transfer to the protonated nucleobase. Hence, by studying hydrogen-rich DNA dinucleotide cation radicals in the gas phase, one can shed light on the intrinsic electronic properties of transient radicals formed in solution.

We now extended the study of DNA dinucleotide cation radicals to involve guanine and cytosine nucleobases, as in $(dGG + 2H)^{+\bullet}$, $(dCG + 2H)^{+\bullet}$, and $(dGC + 2H)^{+\bullet}$. Our goal was to determine the structures of the dication precursors and characterize the hydrogen-rich cation radicals formed by electron transfer using tandem mass spectrometry and UV–vis photodissociation action spectroscopy (UVPD). UVPD is based on resonant absorption of a photon over a scanned range of wavelengths, leading to dissociation to fragment ions. The wavelength-dependent profile of the fragment ion intensities is used to track absorbance of the cation radical, producing an action spectrum, which is analogous to an absorption spectrum.[41,42] The mass-resolved channels of the action spectrum can further provide information on dissociations from particular electronic excited states of the cation radical. Action spectra are assigned to cation radical structures by comparison with absorption spectra obtained by quantum chemistry methods, such as time-dependent density functional theory (TD-DFT)[43] or equation-of-motion coupled clusters calculations.[44] Previous UVPD studies have found a close agreement between the experimental UV–vis action spectra and the calculated absorption spectra for several peptide and nucleobase cation radicals,[31,32,34,45−47] suggesting UVPD action spectroscopy as a powerful tool for structure elucidation of transient radicals. Here, we wish to show by experiment and theory that purine and pyrimidine nucleobases in dinucleotide cation radicals exhibit different properties regarding nucleobase stacking, hydrogen bonds, and propensity for undergoing intramolecular proton transfer.

EXPERIMENTAL SECTION

Materials and Methods. Dinucleotides dGG, dGC, and dCG were custom-synthesized by Integrated DNA Technologies (Coralville, IA) and used as received. Dibenzo-18-crown-6-ether (DBCE, CAS Number 14187-32-7) was purchased from Sigma-Aldrich (Milwaukee, WI). All solvents were of high-performance liquid chromatography analytical grade. Mass spectra were measured on an LTQ-XL-ETD linear ion trap mass spectrometer (Thermo Fisher, San Jose, CA) equipped with an auxiliary chemical ionization source for the production of fluoranthene anions. Doubly charged precursor ions were generated in a home-built micro-electrospray ion source consisting of a fused silica capillary pulled to a 10 μm diameter tip and maintained at 2.2 kV. Methanol/water/acetic acid (50/50/1) solutions containing the dinucleotide and DBCE in a 1:1.2 molar ratio at 10–20 μM concentrations were sprayed at 1.5–2 μL min^{-1} flow rates. $(dGC + DBCE + 2H)^{2+}$ precursor ions were generated from acetonitrile/water/acetic acid (50/50/1) solutions at 10–20 μM concentrations. Electron-transfer dissociation (ETD) mass spectra were obtained by ion–ion charge-transfer reactions with fluoranthene anion radicals at 150–200 ms reaction times. The charge-reduced dinucleotide cation radicals were selected by mass with 2–3 mass unit isolation windows. UVPD was performed as described previously.[45] Briefly, the mass-isolated and trapped ions were irradiated by light pulses (3–6 ns pulse width, 20 Hz repetition rate) produced by an EKSPLA NL301G (Altos Photonics, Bozeman, MT) Nd:YAG laser source equipped with a PG142C optical parametric oscillator.

DOI: 10.1021/acs.jpcb.8b07925
J. Phys. Chem. B 2018, 122, 9665–9680

This provided wavelength tuning in the three ranges, 210−354, 355−400, and 400−700 nm, with a laser power of 0.52−12.69 mJ per pulse. The laser power was measured at each wavelength, typically in 2 nm steps. The intensities of the resulting UVPD MS^3 fragment ions were monitored as a function of wavelength, normalized to the laser output power at each wavelength, and plotted to provide action spectra.

Calculations. Precursor dication structures were obtained for noncovalent complexes with 18-crown-6-ether (CE) as a surrogate for DBCE. Previous structure analysis has indicated very similar structures and relative energies for dication complexes of dAA with CE and DBCE,[34] justifying the use of the smaller CE in the computational analysis of precursor ion structures. Conformation analysis of the dication CE complexes was performed by Born−Oppenheimer molecular dynamics (BOMD) calculations using the semiempirical all-valence-electron PM6 method[48] supplemented with dispersion corrections,[49] PM6-D3H4, and run by MOPAC[50] under the Cuby4 platform,[51] as described previously.[52] Born−Oppenheimer molecular dynamics (BOMD) trajectories were run at 310−410 K using the Berendsen thermostat algorithm.[53] The conformational search was carried out for several protomers of the dinucleotides, as described later in the paper. Selected low-energy conformers from the BOMD runs of each complex protomer were reoptimized by density functional theory (DFT) calculations using the B3LYP[54] and ωB97X-D[55] hybrid functionals. The B3LYP calculations were performed with the 6-31G(d,p) basis set to provide harmonic frequencies that were used to calculate ion enthalpies and entropies at the ion trap temperature (310 K). The ωB97X-D calculations were carried out with the 6-31+G(d,p) basis set to provide the electronic terms. The combined electronic, enthalpy, and entropy terms were combined to produce free energies that were used to rank conformers of each protomeric complex. In addition, solvation energies in water, methanol, and acetonitrile were calculated with ωB97X-D/6-31+G(d,p) using the polarizable continuum model.[56] The lowest-free-energy ions were used for the selection of protomers in the charge-reduced dinucleotide cation radicals. Cation radical structures were optimized by B3LYP, ωB97X-D, and M06-2X[57] calculations with the 6-31+G(d,p) basis set that were run within the spin-unrestricted formalism. Single-point energies were obtained by B3LYP, ωB97X-D, M06-2X, and Møller−Plesset[58] (MP2-(frozen core)) calculations with the larger 6-311++G(2d,p) basis set. High-spin states in spin-unrestricted UMP2 energies were annihilated using the standard procedures[59,60] that reduced the spin expectation values to $\langle S^2 \rangle < 0.76$. Additionally, restricted open-shell (ROMP2) single-point energy calculations were performed to assess the effect of spin contamination on the calculated energies.[61] Atomic spin densities were calculated using the natural population analysis[62] of the M06-2X/6-311++G(2d,p) wave functions. Excitation energies and oscillator strengths were obtained for 45−55 excited states by time-dependent DFT calculations[43] with ωB97X-D and M06-2X/6-31+G(d,p), according to previous benchmarking studies.[31,32] Excited states having spin expectation values $\langle S^2 \rangle > 1.5$ were discarded. All of the electronic structure calculations were performed with the Gaussian 16 (revision A.03) suite of programs.[63] Rice−Ramsperger−Kassel−Marcus (RRKM) calculations of unimolecular rate constants[64] were performed using the QCPE program[65] that was recompiled for Windows 7.[66] Rotations were treated adiabatically, and the rate constants obtained by direct count of quantum states were Boltzmann-averaged over the distribution of ion rotational states at 310 K.

RESULTS

Dinucleotide Cation Radical Generation. Electrospray ionization of dinucleotides dGG, dCG, and dGC produced doubly protonated cations $(dGG + 2H)^{2+}$, $(dCG + 2H)^{2+}$, and $(dGC + 2H)^{2+}$, respectively, which were selected by mass and subjected to ion−ion reactions with fluoranthene anion radicals. Electron transfer to dinucleotide dications resulted in predominant dissociation, yielding only minor fractions of cation radicals. This is illustrated by the electron-transfer dissociation (ETD) mass spectrum of $(dGG + 2H)^{2+}$ (Figure S1) that displayed fragment ions formed by loss of H, nucleobase, and the formation of protonated nucleobases. Hence, ETD of the dinucleotide dications was unsuitable for the generation of stable hydrogen-rich cation radicals. We note that larger oligonucleotides have been shown to form very stable cation radicals upon electron transfer to multiply charged ions, which has been deemed detrimental to using ETD for DNA sequence analysis.[67] To efficiently generate the pertinent cation radicals from dinucleotides, we resorted to a previously employed method, which is based on noncovalent ion−molecule complexes of the dication with crown ethers.[34,68] These are formed as doubly charged ions by electrospray and subjected to ETD. Electron transfer results in charge reduction and elimination of a neutral crown ether molecule, forming intact hydrogen-rich dinucleotide cation radicals in excellent yield. Figure 1a−c illustrates the formation by ETD of $(dGG + 2H)^{+\bullet}$, $(dCG + 2H)^{+\bullet}$, and $(dGC + 2H)^{+\bullet}$ from complexes with dibenzo-18-crown-6-ether (DBCE). With dGG, the doubly charged complex $(dGG + DBCE + 2H)^{2+}$ (m/z 479, Figure 1a) underwent efficient ETD to form the $(dGG + 2H)^{+\bullet}$ cation radical at m/z 598, which was accompanied by minor $(dGG + H)^+$ (m/z 597), $(dGG + DBCE + H)^+$ (m/z 957), and $(DBCE + NH_4)^+$ (m/z 378) fragment ions. Similar results were found for the other dinucleotide complexes.

Cation radicals with cytosine at the 5′-terminus, $(dCG + 2H)^{+\bullet}$, showed a slightly higher propensity for side reactions, such as elimination of H and water, as indicated by the corresponding m/z 557, 517, 540, and 500 fragment ions in the ETD spectra of the complexes (Figure 1b).

Dinucleotide Cation Radical Collision-Induced Dissociation and Photodissociation Spectra. The dinucleotide cation radicals produced by ETD of the crown−ether complexes were selected and isolated by their mass-to-charge ratios and characterized by collision-induced dissociation ($CID\text{-}MS^3$) and photodissociation mass spectra to identify and compare the major fragmentation pathways. For the DNA backbone fragment ion nomenclature, see ref 69. $CID\text{-}MS^3$ of $(dGG + 2H)^{+\bullet}$ resulted in a dominant competitive loss of guanine and $(guanine + H)^\bullet$ radical to give the respective m/z 447 and 446 fragment ions (Figure 2a). Backbone cleavage forming the isobaric d_1 and w_1 ions (m/z 348) and their H-atom adducts (m/z 349) was also observed. $CID\text{-}MS^3$ of $(dGC + 2H)^{+\bullet}$ and $(dCG + 2H)^{+\bullet}$ yielded dramatically different spectra (Figure 2b,c). The cation radical with 3′-cytosine underwent a number of dissociations, including a dominant loss of water (m/z 540), cytosine (m/z 447), and guanine (m/z 406), 3′-deoxyribose cross-ring cleavages (labeled xx, m/z 512, 484, 403, 390), and backbone cleavages with charge retention on the 5′-guanosine fragment (d_1, m/z 348) and 3′-

DOI: 10.1021/acs.jpcb.8b07925
J. Phys. Chem. B 2018, 122, 9665−9680

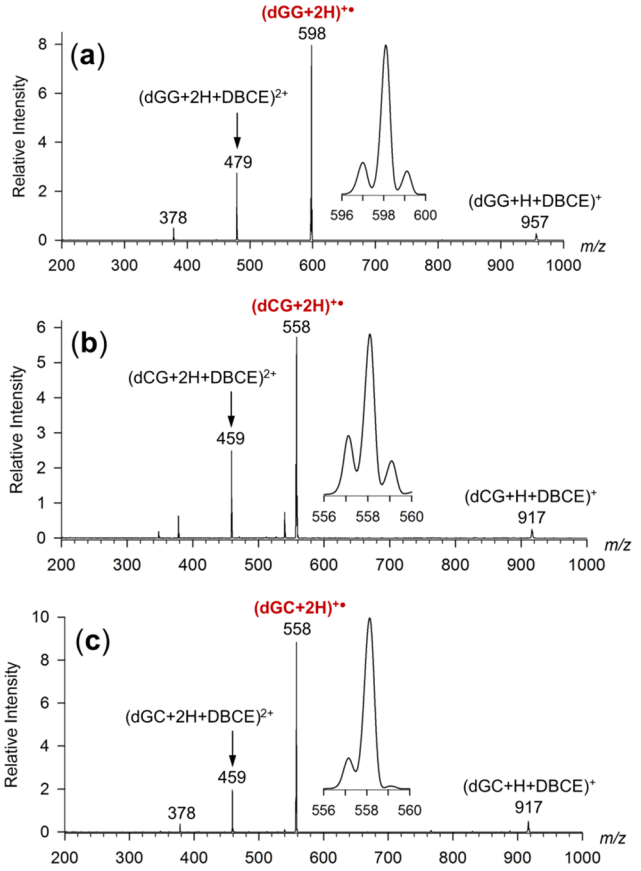

Figure 1. ETD mass spectra (fluoranthene anion, reaction time 150 ms) of dinucleotide dication complexes with dibenzocrown ether (DBCE) (a) $(dGG + DBCE + 2H)^{2+}$, (b) $(dCG + DBCE + 2H)^{2+}$, and (c) $(dGC + DBCE + 2H)^{2+}$.

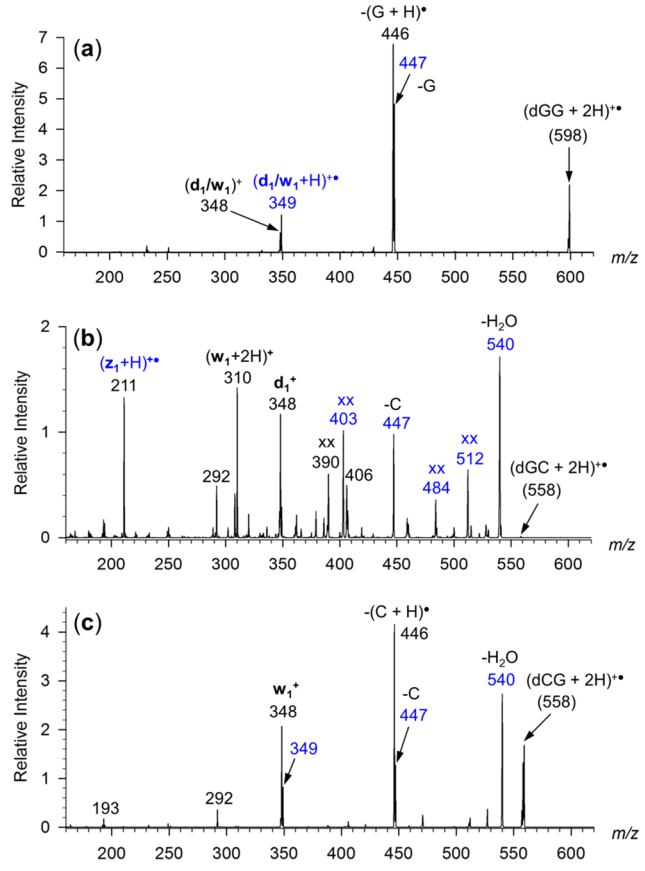

Figure 2. CID-MS^3 spectra of dinucleotide cation radicals: (a) $(dGG + 2H)^{+\bullet}$, (b) $(dGC + 2H)^{+\bullet}$, and (c) $(dCG + 2H)^{+\bullet}$. Cation-radical fragments are labeled blue.

cytidine fragments, $(w_1 + 2H)^+$ (m/z 310), and $(z_1 + H)^{+\bullet}$ (m/z 211). Contrasting this, CID-MS^3 of $(dCG + 2H)^{+\bullet}$ showed major loss of water (m/z 540), (cytosine + H)$^\bullet$ radical (m/z 446), and cytosine (m/z 447), whereas loss of guanine was very minor (m/z 406). Backbone cleavage resulted in the retention of charge on the 3′-guanine fragment (w_1, m/z 348) and its H-atom adduct, $(w_1 + H)^{+\bullet}$, at m/z 349. The cation-radical dissociations allowed us to deduce some common features of the nucleobase nature and position affecting the spectra. First, a cytosine at the 3′-terminus was highly conducive to facile elimination of water (Figure 2b). Second, a cytosine at the 5′-terminus was chiefly lost as a hydrogen adduct radical (Figure 2c) rather than a molecule. Third, the loss of cytosine outcompeted loss of guanine. Finally, the cytosine fragments effectively competed for the charging proton when the nucleobase was at the 3′-terminus (Figure 2c).

Photodissociation of the dinucleotide cation radicals produced fragment ions that were similar to those observed by CID. This is illustrated by UVPD mass spectra obtained at 280 nm, where $(dGG + 2H)^{+\bullet}$, $(dCG + 2H)^{+\bullet}$, and $(dGC + 2H)^{+\bullet}$ exhibited strong absorption (Figure S2a–c, Supporting Information). UVPD of $(dGG + 2H)^{+\bullet}$ resulted in loss of guanine and (guanine + H)$^\bullet$ radicals (m/z 447 and 446, respectively) and formation of backbone d_1/w_1 fragment ions and their hydrogen adducts (m/z 348, 349, Figure S2a). UVPD of $(dCG + 2H)^{+\bullet}$ resulted in loss of cytosine and (cytosine + H)$^\bullet$ radicals, and the formation of backbone 5′-guanine containing w_1 ions (m/z 348), indicating prevalent dissociation in the cytidine moiety (Figure S2b). UVPD of $(dGC + 2H)^{+\bullet}$ gave rise to several fragment ions, namely, m/z 447 (loss of C), m/z 403 (cross-ring fragment), m/z 310 (w_1 + 2H), and m/z 308 (w_1 − 2H) (Figure S2c). It should be noted that strong absorption at 280 nm resulting in photodissociation was also observed for closed-shell cations $(dGG + H)^+$, $(dCG + H)^+$, dications $(dGG + 2H)^{2+}$, and $(dCG + 2H)^{2+}$, as evidenced by the respective ion action spectra (Figures S3 and S4, Supporting Information). Similar absorption has been reported for aqueous dG-5′-phosphate.[70,71] Thus, electronic excitation at 280 nm in the gas-phase cation radicals cannot be unambiguously assigned to chromophores associated with the nucleobase radical moieties.

$(dGG + 2H)^{+\bullet}$ Action Spectroscopy and Ion Structures. The main photodissociation fragment ions were used to monitor absorption by the gas-phase cation radicals in the 210–700 nm region of the spectrum. Starting with $(dGG + 2H)^{+\bullet}$, the cation radical displayed a long-wavelength band at 450–470 nm that was composed of contributions from all major dissociation channels (Figure 3a). The mass-resolved channels showed a slightly shifted absorption maxima that appeared at 450 nm for m/z 446 and 349, whereas at 470 nm for m/z 447 and 348. The action spectrum further showed two bands at 330 and 310 nm and a major band centered at 270 nm. The latter band was chiefly composed of contributions from the dissociation channels by loss of G and (G + H)$^\bullet$ radical. The backbone dissociations forming the $(d_1/w_1)^+$ and $(d_1/w_1 + H)^{+\bullet}$ fragment ions gave a band that was slightly

DOI: 10.1021/acs.jpcb.8b07925
J. Phys. Chem. B 2018, 122, 9665–9680

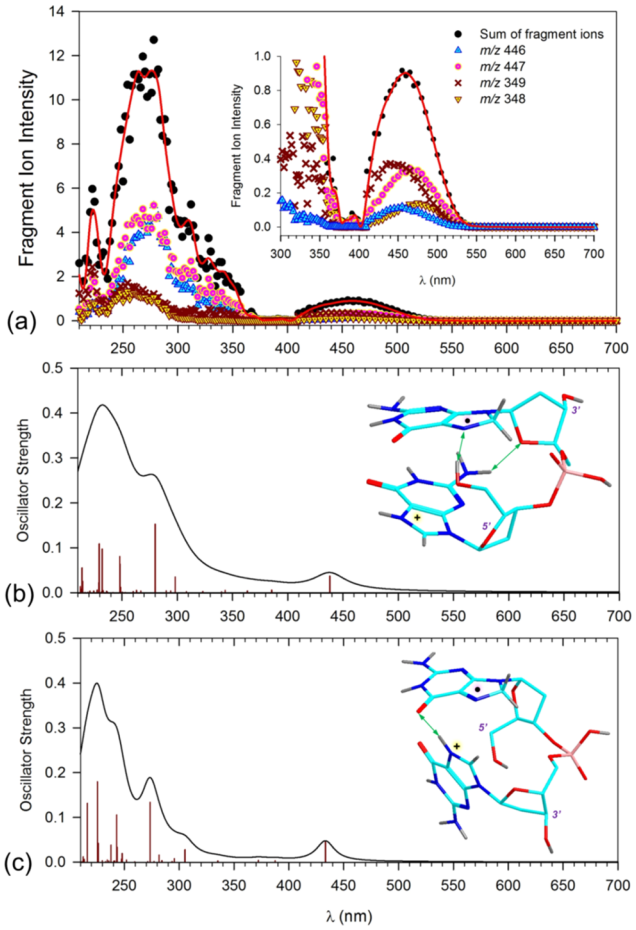

Figure 3. (a) Photodissociation action spectrum of $(dGG+2H)^{+\bullet}$. The inset shows an expanded 300−700 nm region. M06-2X/6-31+G(d,p) TD-DFT calculated absorption spectra of (b) **GG1e**$^{+\bullet}$ and (c) **GG1f**$^{+\bullet}$. The bars represent the calculated absorption wavelengths and oscillator strength. The band shapes are from artificial line broadening with Lorenztian functions at 12 nm full width at half-maximum.

blue-shifted, peaking at 260 nm. Another band appeared at 210 nm, which received contributions from all major dissociation channels.

To aid interpretation of the action spectra, we carried out extensive calculations of structures and energies of dication precursors and cation radicals. A detailed study of the dication−crown complexes was necessary to identify low-energy dinucleotide protomers that could be expected to be formed by electrospray. The $(dGG+2H)^{2+}$ cations are discussed first. With dGG, we considered structures with nucleobases protonated at N-7 of the canonical tautomer, which is the most basic position in guanine.[72−74] Another set had the 6-OH tautomer of guanine protonated at N-3, which is the second most basic position.[72] The crown ether ligand was coordinated by the 3′- or 5′-nucleobase cations of either protomeric type. As established previously for dAA complexes,[34] coordination of dibenzo-18-crown-6-ether is very similar to that of 18-crown-6-ether and can be established by computations for complexes of the latter as surrogates. BOMD of these protomers and crown−ether positional isomer combinations, followed by DFT optimization yielded structures that were ranked by free energy. Several low-free-energy structures were reoptimized with ωB97X-D, including polarizable continuum model to estimate solvation energies of the complexes in water and acetonitrile (Table S1, Supporting Information). The lowest-free-energy structures of each type are depicted in Figures 4 and S5 (Supporting Information).

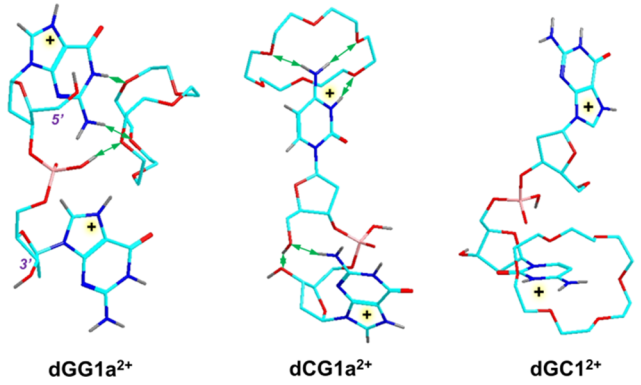

Figure 4. Lowest-free-energy dication dinucleotide−crown−ether complexes from ωB97X-D/6-31+G(d,p) geometry optimizations. Atom color coding is as follows: cyan = C, blue = N, red = O, orange = P, gray = H. Only exchangeable and nucleobase hydrogens are shown.

Among the positional isomers, those having the crown ether ligand at the 5′-terminus were consistently more stable than the 3′-terminus isomers. According to DFT calculations, the canonical N-7 protonated ion **dGG1a**$^{2+}$ and its conformer **dGG1b**$^{2+}$ were the most stable structures in both the gas phase and solution (Table S1).

The structures combining N-7 protonation on one guanine with N-3 protonation of the 6-OH enol tautomer of the other guanine (**dGG2**$^{2+}$ and **dGG3**$^{2+}$, respectively) were close enough in energy to be considered as potential candidates for $(dGG+2H)^{+\bullet}$ cation radicals produced by ETD.

Electron transfer to **dGG1**$^{2+}$ followed by crown−ether loss can be viewed as originally producing cation radical **dGG1a**$^{+\bullet}$ in which the nucleobases were remote and the incoming electron was attached to the 5′-nucleobase (Scheme 2). Interestingly, attempts to fix the radical within the 3′-guanine nucleobase by puckering the ring in the initial guess geometry resulted in a relaxation upon gradient geometry optimization, yielding local energy minima that were 5′-guanine radicals. The calculated relative energies of $(GG+2H)^{+\bullet}$ cation radicals are displayed in Table 1. In a further conformational search, ion **dGG1a**$^{+\bullet}$ underwent a highly exothermic folding to form conformer **dGG1b**$^{+\bullet}$, in which the radical and cation guanine nucleobases were stacked. The further development of this structure likely involved a proton transfer between the N-7 and C-8 guanine positions in **dGG1b**$^{+\bullet}$ that was relayed by the 5′-OH group and proceeded through a low-energy transition state (**dGG-TS1**), exothermically yielding an isomeric cation radical **dGG1c**$^{+\bullet}$. The latter isomer can further refold to other low-energy structures, such as **dGG1d**$^{+\bullet}$ or its rotamer **dGG1g**$^{+\bullet}$. As a result of the proton transfer, ions **dGG1c**$^{+\bullet}$, **dGG1d**$^{+\bullet}$, and **dGG1g**$^{+\bullet}$ had 3′-guanine as a neutral moiety, whereas 5′-nucleobase was turned into a 7,8-dihydroguanine cation radical (Scheme 2). An inverse proton transfer from 5′-7,8-dihydroguanine to N-7 of the 3′-nucleobase can form isomer **dGG1e**$^{+\bullet}$ with a reversed position of the neutral radical and cation nucleobase moieties. We also considered an alternative isomerization process resulting in the formation of a 3′-guanine

DOI: 10.1021/acs.jpcb.8b07925
J. Phys. Chem. B 2018, 122, 9665−9680

Scheme 2. Formation of $(GG + 2H)^{+\bullet}$ Cation Radicals[a]

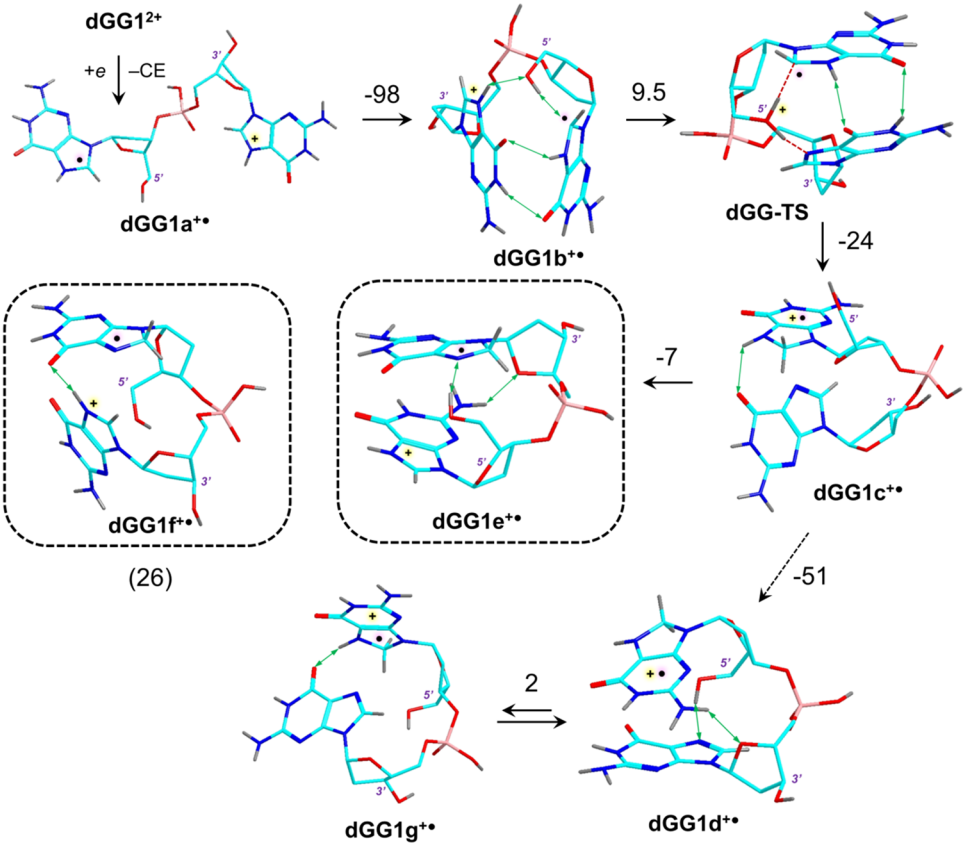

[a]Reaction enthalpies (kJ mol^{-1}) are from M06-2X/6-311++G(2d,p) calculations including zero-point vibrational energies and refer to 0 K. For energies from other calculations, see Table 1.

radical and 5′-cation (**dGG1f**$^{+\bullet}$), representing another low-energy isomer.

TD-DFT calculations of excitation energies and oscillator strength in **dGG1a**$^{+\bullet}$**–dGG1f**$^{+\bullet}$ provided the absorption spectra (Figure S6) to be compared to the experimental action spectrum (Figure 3a). The calculated spectra of the low-energy isomers **dGG1c**$^{+\bullet}$, **dGG1d**$^{+\bullet}$, and **dGG1g**$^{+\bullet}$ having the 7,8-dihydroguanine cation radical chromophore (Figure S6) did not display the prominent 450–470 nm band shown in the action spectrum while having a band at 380–390 nm that was absent in the action spectrum. In contrast, the calculated spectra of isomers **dGG1e**$^{+\bullet}$ and **dGG1f**$^{+\bullet}$ were compatible with the action spectrum, showing bands at 240, 280–300, and 433–438 nm (Figure 3b,c). It should be noted that the action spectrum was obtained at the ion trap temperature (310 K), whereas the TD-DFT calculated bands correspond to vertical excitation in 0 K structures. Vibronic broadening due to electronic excitations from vibrationally excited states present at 310 K is expected to both broaden the bands and red-shift the absorption maxima by 10–30 nm,[75] as observed previously for nucleobase[31,32] and dinucleotide cation radicals.[34]

The nature of the diagnostic transition giving rise to the 450–460 nm band was elucidated by analyzing the molecular orbitals involved in the electron excitations in **dGG1e**$^{+\bullet}$ and **dGG1f**$^{+\bullet}$ (Figure 5). In both these radicals, the pertinent transitions corresponded to the first (A) excited state. The transitions in **dGG1e**$^{+\bullet}$ occurred from the singly occupied π-molecular orbital (SOMO, 156α) to a combination of π^* orbitals, all located at the 3′-guanine radical. Charge transfer to the π-electron system of the 5′-guanine cation was very minor. The transitions in **dGG1f**$^{+\bullet}$ occurred from the π-SOMO located at the 5′-radical to a combination of π^* orbitals chiefly located at the same ring. In addition, the A excited state in **dGG1f**$^{+\bullet}$ involved a small portion of electron transfer to the protonated imidazole ring of the 3′-guanine cation (Figure 5).

The assignment of the excited states in $(GG + 2H)^{+\bullet}$ was further corroborated by TD-DFT calculations of a model 7,8-dihydroguanosine radical, $(G + H)^{\bullet}$, having an analogous π-electron system (Figure S7, Supporting Information). In particular, the TD-DFT absorption spectrum of $(G + H)^{\bullet}$ displayed a prominent band at 439 nm, which was analogous to the 438 and 433 nm bands of **dGG1e**$^{+\bullet}$ and **dGG1f**$^{+\bullet}$, respectively. With $(G + H)^{\bullet}$, we were able to obtain a TD-DFT spectrum that was broadened by including 600 vibronic transitions at 310 K to estimate the thermal shift and broadening of the nucleobase bands. In particular, the 439 nm band corresponding to excitation to the first excited state exhibited a substantial red shift and broadening (Figure S7).

In addition to N-7-diprotonated guanine tautomers, we also considered cation radicals originating from the N-7, N-3-protonated O-6 enol isomers **dGG2**$^{2+}$ and **dGG3**$^{2+}$. However, none of these cation radicals (**dGG1b**$^{+\bullet}$**–dGG1f**$^{+\bullet}$, **dGG2a**$^{+\bullet}$, **dGG2b**$^{+\bullet}$, **dGG3a**$^{+\bullet}$, **dGG3b**$^{+\bullet}$ **dGG4a**$^{+\bullet}$, and **dGG4b**$^{+}$) provided a match with the experimental action spectrum (for spectra and discussion, see Figures S6, S8, and S9 in the Supporting Information). Hence, we concluded that these low-energy cation radicals were not produced by electron transfer in the gas phase.

DOI: 10.1021/acs.jpcb.8b07925
J. Phys. Chem. B 2018, 122, 9665–9680

Table 1. Relative Energies of $(dGG + 2H)^{+\bullet}$ Ions

Ion	Relative Energy[a,b] B3LYP	B97X-D[c]	M06-2X[c]	PMP2[c]	ROMP2[c]
dGG1a$^{+\bullet}$	56	-	98	129	-
dGG1b$^{+\bullet}$	0	0	0	0	0
dGG1c$^{+\bullet}$	–39	–19	–24	–16	–25
dGG1d$^{+\bullet}$	–46	–72	–75	–80	–88
dGG1e$^{+\bullet}$	–9	–32	–30	–31	–31
dGG1f$^{+\bullet}$	–15	3	2	24	22
dGG2a$^{+\bullet}$	114	68	107	-	-
dGG2b$^{+\bullet}$	68	55	74	-	-
dGG3a$^{+\bullet}$	61	75	66	-	-
dGG3b$^{+\bullet}$	35	57	55	-	-
dGG4a$^{+\bullet}$	–32	–19	–20	2	–8
dGG4b$^{+\bullet}$	–29	–49	–41	–23	–32
dGG-TS	6	12	9	–9	–19
dGG1f$^{+\bullet}$ → loss of G	147[d]	205[d]	201[d]	189[d]	187[d]
dGG1f$^{+\bullet}$ → loss of (9H-G)$^{\bullet}$	77[e]	146[e]	140[e]	137[e]	155[e]
dGG1f$^{+\bullet}$ → loss of (3H-G)$^{\bullet}$	176[f]	251[f]	243[f]	233[f]	252[f]

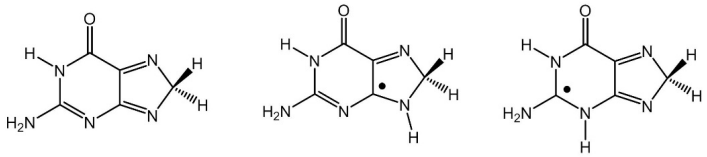

G 9H-G$^{\bullet}$ 3H-G$^{\bullet}$

[a]In kJ mol^{-1}. [b]Including B3LYP/6-31+G(d,p) zero-point vibrational corrections. [c]Single-point calculations with the 6-311++G(2d,p) basis set. [d]Relative to **dGG1f**$^{+\bullet}$. [e]Formation of the 8,9-dihydroguanine radical $(9H\text{-}G)^{\bullet}$. [f]Formation of the 3,8-dihydroguanine radical $(3H\text{-}G)^{\bullet}$.

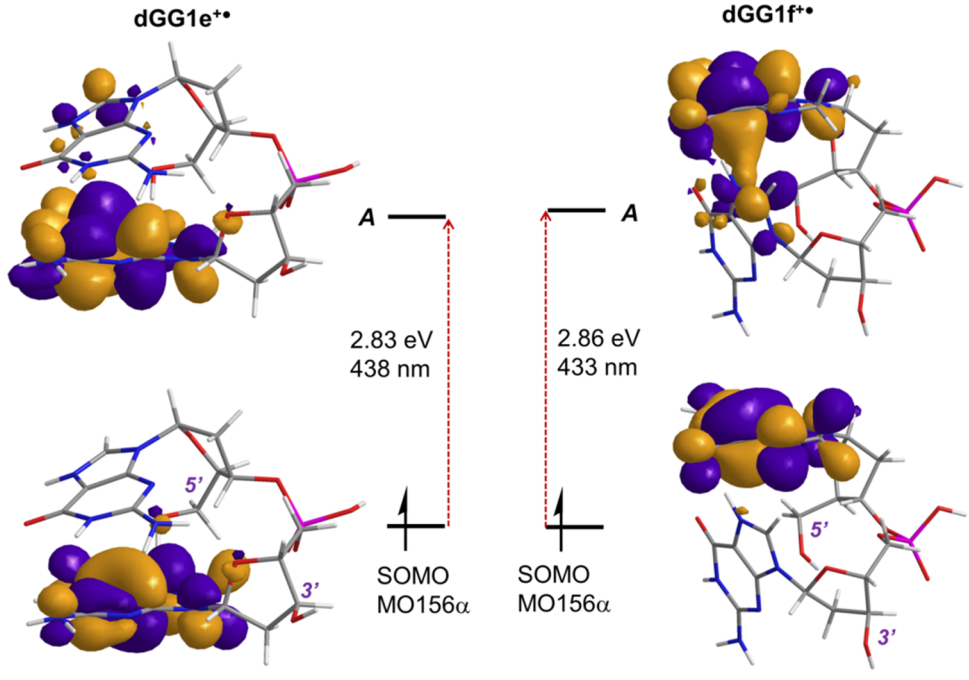

Figure 5. Molecular orbitals for the first excited state of $(dGG + 2H)^{+\bullet}$.

DOI: 10.1021/acs.jpcb.8b07925
J. Phys. Chem. B 2018, 122, 9665−9680

Scheme 3. Dissociations of dGG1f$^{+\bullet}$ by Loss of G and (G + H)$^{\bullet}$ [a]

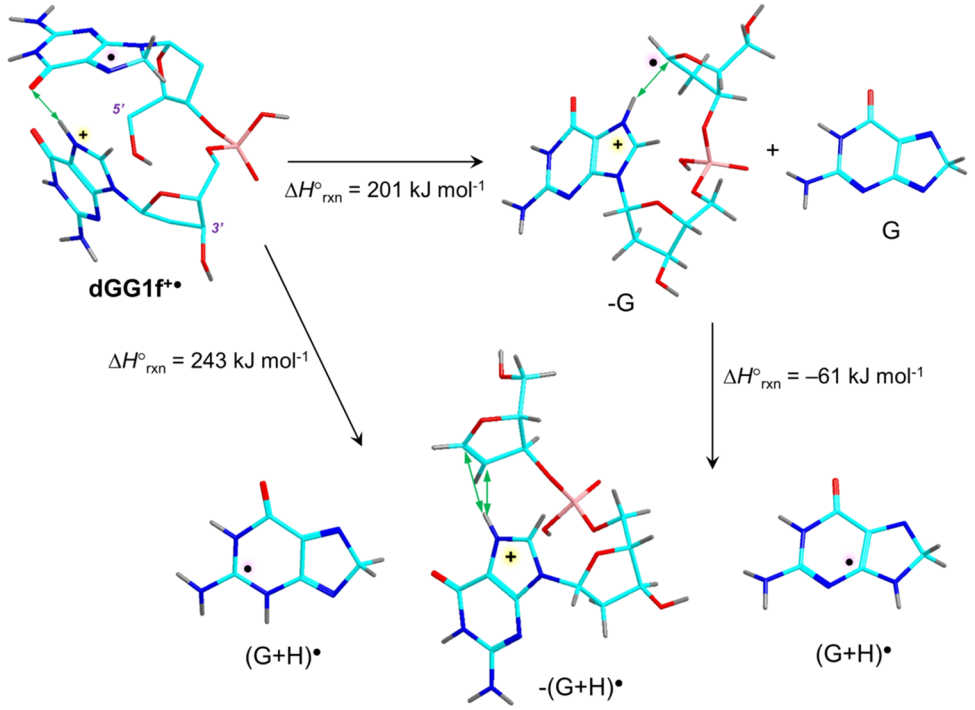

[a]Reaction step enthalpies, ΔH°_{rxn}, kJ mol^{-1}, are from M06-2X/6-311++G(2d,p) calculations and refer to 0 K.

To summarize the structure assignment of (GG + 2H)$^{+\bullet}$ ions, the 7-H-guanine protomers in the cation radicals initially produced by ETD were determined by the protonation sites in the lowest-energy crown−ether complex **dGG1a**$^{2+}$ that was expected to dominate in both solution and gas phase. Favored protonation at both N-7 positions in **dGG1a**$^{2+}$ was consistent, with N-7 being the most basic site in guanine,[72] and gas-phase 2′-deoxyguanosine.[74] Charge reduction resulted in a major change of structure. Loss of Coulomb repulsion triggered exothermic nucleobase stacking that was followed by combined N-7-proton transfers yielding 8,8-H guanine radicals that showed a signature absorption band in the action spectrum. The position of the guanine radical at the 3′- or 5′-terminus could not be unequivocally determined from the action spectrum alone. However, energy considerations favored isomer **dGG1e**$^{+\bullet}$ with a 3′-guanine radical.

To gauge the range of photon energies capable of causing single-photon photodissociation of (dGG + 2H)$^{+\bullet}$ cation radicals, we calculated the dissociation energies for loss of guanine and (G + H)$^{\bullet}$ radical from **dGG1f**$^{+\bullet}$. The departing guanine molecule was considered as a less stable C-8−H_2 tautomer, which originated by direct cleavage of the 5′-guanine radical moiety in **dGG1f**$^{+\bullet}$. Likewise, the (G + H)$^{\bullet}$ radical was taken as a C-8−H_2 tautomer (Scheme 3). The loss of guanine had a threshold energy of 187−205 kJ mol^{-1} at different levels of theory (Table 1). The loss of (G + H)$^{\bullet}$ was found to be kinetically competitive and can be presumed to have a similar threshold energy. In our energy analysis, we considered the molar enthalpy of **dGG1f**$^{+\bullet}$ at 310 K (106 kJ mol^{-1}) and an estimated kinetic shift of 120 kJ mol^{-1} for the dissociation to occur on the 50 ms ion trap time scale. Hence, excitation of approximately 200 + 120 − 105 = 215 kJ mol^{-1} should be sufficient to drive dissociation. Such energy can be supplied by a single photon of λ < 550 nm. This indicated that the bands observed in the action spectrum of (dGG + 2H)$^{+\bullet}$ (Figure 3a) could be produced by single photon absorption.

(dCG + 2H)$^{+\bullet}$ Action Spectroscopy and Ion Structures. The action spectrum of (dCG + 2H)$^{+\bullet}$ showed a weak band at 450−480 nm and a stronger one at 350 nm that were chiefly composed of contributions from the sequence d_1 fragment ions (m/z 348 and 349, Figure 6a). Another strong band at 280 nm had a major contribution from the m/z 446 fragment ions formed by loss of the (C + H)$^{\bullet}$ radical. To identify the (dCG + 2H)$^{+\bullet}$ isomers with matching absorption spectra, we first carried out extensive analysis of the (dCG + crown + 2H)$^{2+}$ precursor ions with the goal of sorting out by energy the guanine and cytosine ion tautomers as well as isomers differing in the position of the crown ligand. In addition to the above-mentioned guanine protonation tautomers, cytosine protonation was considered at the O-2 and N-3 positions which are the most and nearly equally basic sites in cytosine.[72,76,77] BOMD trajectories followed by full optimization with ωB97X-D/6-31+G(d,p) yielded low-energy gas-phase and solvated structures for several combinations of protomers and crown−ether complexes (Figure S10) (Table S2, Supporting Information). The energy data indicated a favorable formation of N-3-protonated cytosine at the 5′-terminus, which coordinated the crown ether, while the 3′-guanine was protonated at N-7, as in **dCG1a**$^{2+}$ (Figure 4) and its conformers **dCG1b**$^{2+}$ and **dCG1c**$^{2+}$. Of the other protomeric and positional combinations (**dCG2**$^{2+}$−**dCG5**$^{2+}$, Figure S10), the only one that was energetically competitive was the positional isomer **dCG2**$^{2+}$ having the same nucleobase protonation pattern as did **dCG1a**$^{2+}$ but with the crown−ether coordination switched to the 3′-guanine ion.

Electron attachment to **dCG1a**$^{2+}$ followed by crown−ether loss produced a cation radical (**dCG1**$^{+\bullet}$) with the unpaired electron occupying the cytosine base (Figure 6b). An alternative structure having the unpaired electron in the

DOI: 10.1021/acs.jpcb.8b07925
J. Phys. Chem. B 2018, 122, 9665−9680

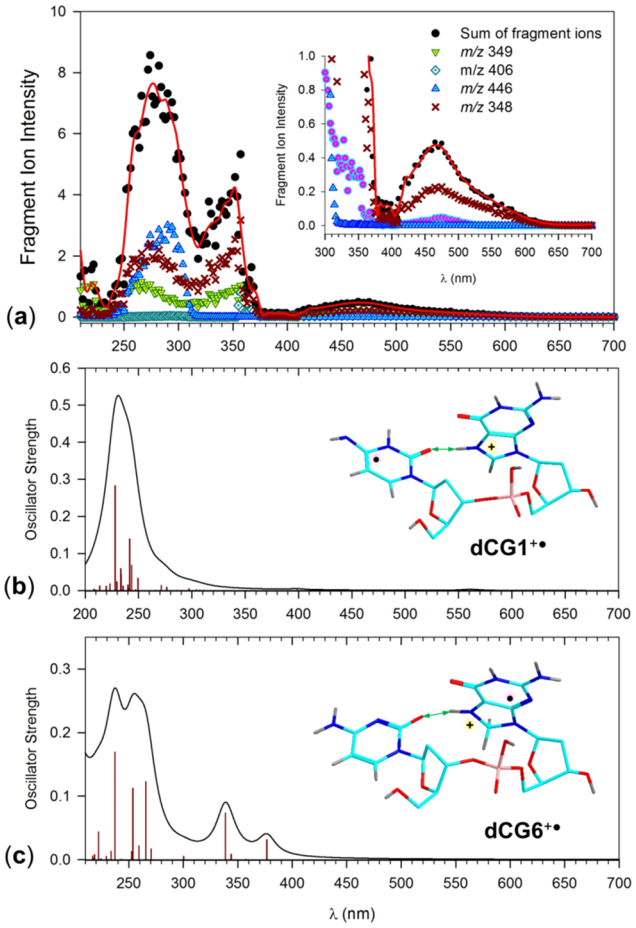

Figure 6. (a) Action spectrum of $(dCG + 2H)^{+\bullet}$. The inset shows the expanded region of 300−700 nm. M06-2X/6-31+G(d,p) TD-DFT absorption spectra of (b) **dCG1**$^{+\bullet}$ and (c) **dCG6**$^{+\bullet}$. The bars show the wavelengths and oscillator strength of the calculated transitions. The band shapes were obtained by convoluting the lines with Lorentzian functions at 12 nm full width at half-maximum.

guanine ring (**dCG2**$^{+\bullet}$, Figure S11a) was a high-energy species corresponding to an excited electronic state of **dCG1**$^{+\bullet}$. For the calculated relative energies of $(CG + 2H)^{+\bullet}$ ions, see Table 2. Other alternative structures were derived from **dCG1**$^{+\bullet}$ by proton or hydrogen atom migrations (Scheme 4).

This produced an O, N-7-dihydroguanine cation radical (**dCG3**$^{+\bullet}$, Figure S11b), O, N-3-dihydrocytosine cation radical (**dCG4**$^{+\bullet}$, Figure S11c), a guanine protonation isomer **dCG5**$^{+\bullet}$ (Figure S11d), and a 7,8-dihydroguanine cation radical (**dCG6**$^{+\bullet}$, Figure 6c). With the exception of the last structure, all of these isomers were less stable than **dCG1**$^{+\bullet}$, so there was no thermodynamic drive for isomerizations forming them. Isomerization of **dCG1**$^{+\bullet}$ to **dCG6**$^{+\bullet}$ was exothermic and involved a transition state (**dCG-TS1**) that was at 98−106 kJ mol^{-1} relative to **dCG1**$^{+\bullet}$ according to different levels of theory (Table 2).

Comparing the action spectrum of $(CG + 2H)^{+\bullet}$ with the calculated absorption spectra of **dCG1**$^{+\bullet}$−**dCG6**$^{+\bullet}$, we found no complete agreement for any single isomer (Figures 6b,c and S11a−d). However, the weak band at 450 nm in the spectrum of **dCG1**$^{+\bullet}$ (Figure 6b) and the bands at 339 and 377 nm in the spectrum of the lowest-energy isomer **dCG6**$^{+\bullet}$ (Figure 6c) could account for the 470 and 350 nm diagnostic features in the action spectrum. Hence, we assigned the action spectrum to a mixture of these two isomers as the closest match. We note that electron transfer to the precursor dication exothermically formed **dCG1**$^{+\bullet}$ as a primary product, which was connected to **dCG6**$^{+\bullet}$ via **dCG-TS1**, thus allowing isomerization if kinetically feasible. To assess the isomerization kinetics, we carried out RRKM calculations that provided unimolecular rate constants (k, s^{-1}) as a function of internal energy (Figure S12a). The calculated rate constants for the rearrangement in **dCG1**$^{+\bullet}$ displayed a slow rise with the ion internal energy. According to the ωB97X-D-based calculations, 10% conversion on the experimental 50 ms time scale was achieved at 310 kJ mol^{-1} internal energy, whereas 50% conversion required 360 kJ mol^{-1} (Figure S12b). Considering the ion thermal energy (E_{therm} = 102 kJ mol^{-1} at 310 K), isomerization via **dCG-TS1** would require >200 kJ mol^{-1} additional excitation in **dCG1**$^{+\bullet}$ acquired by ETD. The excitation in **dCG1**$^{+\bullet}$ (E_{exc}) was estimated as a fraction of the ETD exothermicity that was partitioned in a 0.57:0.43 ratio between **dCG1**$^{+\bullet}$ and the departing DBCE according to their heat capacities. ETD exothermicity (ΔE_{ETD}) was estimated on the basis of the calculated recombination energy of the precursor complex dication (RE = 520 kJ mol^{-1}), fluoranthene electron affinity (EA = 61 kJ mol^{-1}),[78] and the binding energy of DBCE in the reduced complex (E_{dis} = 130 kJ mol^{-1}) as ΔE_{ETD} = (RE − EA − E_{dis}) ≈ 330 kJ mol^{-1}, from which we obtained E_{exc} = 0.57 × ΔE_{ETD} = 188 kJ mol^{-1}. Hence, the estimated internal energy of **dCG1**$^{+\bullet}$, E_{int} = E_{exc} + E_{therm} = 188 + 102 = 290 kJ mol^{-1}, fell close to the kinetically relevant energy region (Figure S12b), allowing partial isomerization to proceed on the ion trap time scale. This analysis was consistent with the action spectrum of $(CG + 2H)^{+\bullet}$ that indicated the formation of a mixture of **dCG1**$^{+\bullet}$ and **dCG6**$^{+\bullet}$.

CID and UVPD of $(dCG + 2H)^{+\bullet}$ showed an abundant loss of cytosine and $(C + H)^{\bullet}$ radicals (Figure 2c). We estimated the pertinent dissociation threshold energies by calculations carried out for isomer **dCG1**$^{+\bullet}$ having a radical cytosine ring. The neutral cytosine molecule was taken as the less stable N-3−H tautomer (iso-C), whose structure correlates with that of the cytosine nucleobase in **dCG**$^{+\bullet}$. The presumed $(C + H)^{\bullet}$ radical product was the most stable N-1−H, N-3−H tautomer (Scheme S1 Supporting Information). The calculated dissociation energies indicated very similar thresholds for loss of iso-C and $(C + H)^{\bullet}$, E_{diss} = 145 and 137 kJ mol^{-1}, respectively (Table 2). Dissociations by loss of C and $(C + H)^{\bullet}$ were notably less endothermic than those by loss of G and $(G + H)^{\bullet}$ (vide supra). This was consistent with the CID and UVPD-MS^3 spectra of $(dCG + 2H)^{+\bullet}$, which showed a nearly exclusive loss of $(C + H)^{\bullet}$ and C (Figures 2 and S2, Supporting Information).

$(dGC + 2H)^{+\bullet}$ Action Spectroscopy and Ion Structures. The action spectrum of $(dGC + 2H)^{+\bullet}$ (Figure 7a) was different from the spectra of both $(dGG + 2H)^{+\bullet}$ and $(dCG + 2H)^{+\bullet}$. Extremely weak broad bands at 620 and 420−500, and 360 nm resulted from contributions of all major dissociation channels. In the short-wavelength region of the spectrum, there was a single strong band carried by all major channels with a maximum at 285 nm. This band had an asymmetric profile, possibly indicating an overlapping minor band with an absorption maximum at 250−260 nm. The 620 and 420−500 nm bands were likely associated with nucleobase radical chromophores that showed similar maxima albeit different intensities for $(dGG + 2H)^{+\bullet}$ and $(dCG + 2H)^{+\bullet}$. The 285 nm band was likely associated with excitations in the radical

DOI: 10.1021/acs.jpcb.8b07925
J. Phys. Chem. B 2018, 122, 9665−9680

Table 2. Relative Energies of $(dCG + 2H)^{+\bullet}$ Ions

	Relative Energy[a,b]				
Ion	B3LYP[c]	B97X-D[c]	M06-2X[c]	PMP2[c]	ROMP2[c]
dCG1$^{+\bullet}$	0	0	0	0	0
dCG2$^{+\bullet}$	-[d]	127	123	-	-
dCG3$^{+\bullet}$	26	30	18	31	17
dCG4$^{+\bullet}$	35	26	11	28	27
dCG5$^{+\bullet}$	66	65	55	-	-
dCG6$^{+\bullet}$	–31	–23	–23	–9	–9
dCG7$^{+\bullet}$	19	23	11	34	42
dCG-TS1	131	103	106	98	101
dCG-TS2	92	54	58	70	76
dCG-TS3	186	194	189	180	171
loss of isoC	109	148	145	165	171
loss of $(C+H)^{\bullet}$	97	141	137	159	161

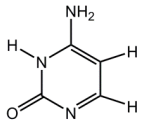

isoC

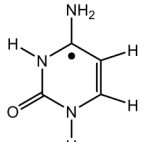

$(C+H)^{\bullet}$

[a]In kJ mol^{-1}. [b]Including B3LYP/6-31+G(d,p) zero-point vibrational corrections. [c]Single-point calculations with the 6-311++G(2d,p) basis set. [d]Collapsed to **dCG1** upon B3LYP/6-31+G(d,p) gradient geometry optimization.

Scheme 4. Isomerization of $(dCG + 2H)^{+\bullet}$ Cation Radicals[a]

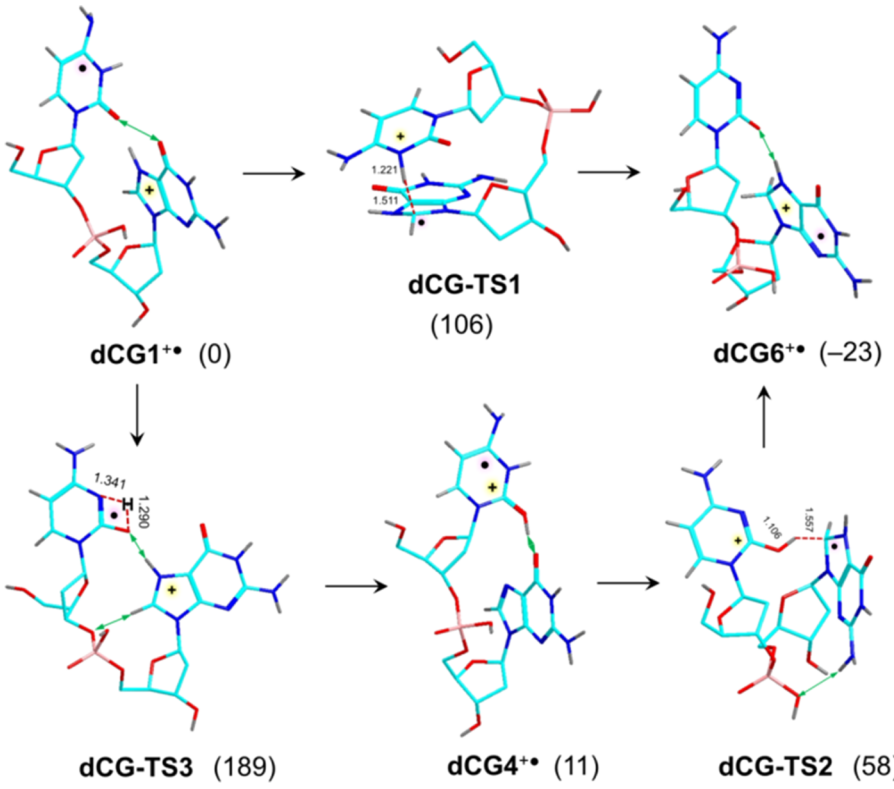

[a]Relative energies (kJ mol^{-1}) are from M06-2X/6-311++G(2d,p) calculations including zero-point vibrational energies and refer to 0 K. For energies from other calculations, see Table S4, Supporting Information.

DOI: 10.1021/acs.jpcb.8b07925
J. Phys. Chem. B 2018, 122, 9665–9680

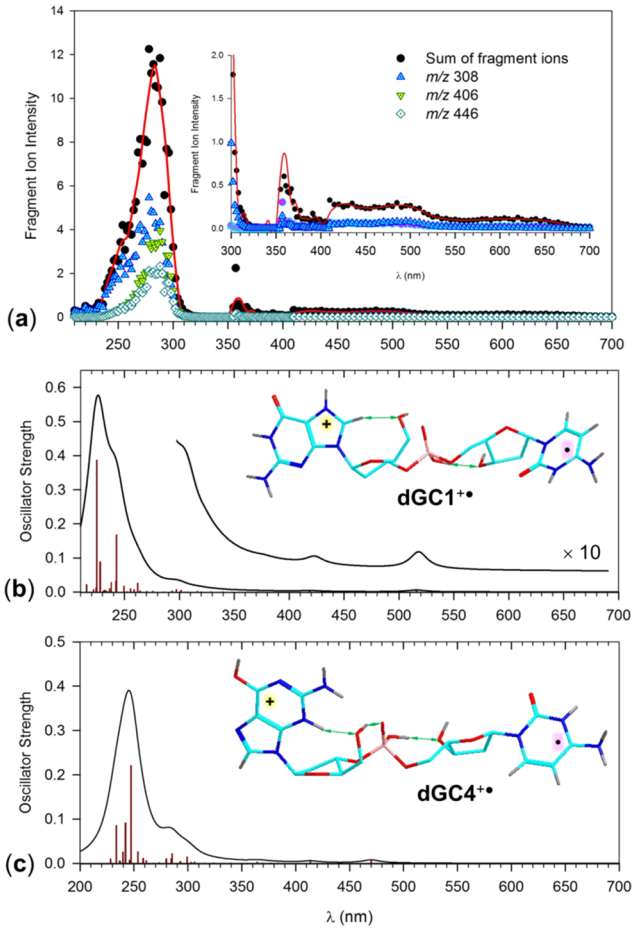

Figure 7. (a) Action spectrum of $(dGC + 2H)^{+\bullet}$. The inset shows the expanded region of 300−700 nm. M06-2X/6-31+G(d,p) TD-DFT absorption spectra of (b) **dGC1**$^{+\bullet}$ and (c) **dGC4**$^{+\bullet}$. The bars show the wavelengths and oscillator strength of the calculated transitions. The band shapes were obtained by convoluting the lines with Lorentzian functions at 12 nm full width at half-maximum.

nucleobase rings, as well as those not affected by radical addition. To provide a more specific interpretation of the action spectra, we carried out calculations of ion structures and excitation energies.

Several $(dGC+CE + 2H)^{2+}$ structures were considered as dication precursors, which were protonated at the basic positions of guanine (N-7 and O-6, N-3) and cytosine (N-3 and O-2) and differed in the location of the crown−ether ligand. All of the dGC protomer types (**GC1**$^{2+}$−**GC8**$^{2+}$, Figure S13) favored crown−ether coordination on the protonated 3′-cytosine ring. BOMD conformational analysis followed by ωB97X-D geometry optimization yielded the lowest-energy gas-phase structures (**GC1**$^{2+}$−**GC5**$^{2+}$). These ions were cytosine N-3-protonated, whereas the guanine was either 6-oxo-N-7−H or 6-OH−N-3−H tautomer. Structure **GC1**$^{2+}$ was the global energy minimum (Figure 4). The free-energy differences notably increased upon including solvation energy in the calculations, making **GC1**$^{2+}$ the by far lowest-energy structure (Table S3). Hence, according to the gas-phase and solvation energy data, **GC1**$^{2+}$ should be formed preferentially by electrospray.

Electron transfer to **dGC1**$^{2+}$ followed by crown−ether ligand loss produced a cytosine radical (**dGC1**$^{+\bullet}$) as a lowest-energy conformer of this structural type (Figure 7b). Ion **dGC1**$^{+\bullet}$ had an extended conformation that did not display nucleobase stacking. The TD-DFT absorption spectrum of **dGC1**$^{+\bullet}$ displayed strong bands in the 235−260 nm region, a weak band at 300 nm and very weak bands at 420 and 515 nm. The overall absorption pattern of **dGC1**$^{+\bullet}$ agreed with that observed in the action spectrum, when allowing for wavelength shifts and band broadening because of vibronic effects. A similar absorption spectrum (Figure 7c) was calculated for the guanine O-6, N-3−H tautomer **dGC4**$^{+\bullet}$ which was another cytosine radical with an extended conformation. Isomer **dGC4**$^{+\bullet}$ was marginally (14−17 kJ mol^{-1}) less stable than **dGC1**$^{+\bullet}$ according to all our calculations (Table 3). For the absorption spectra of the other low-energy isomers **dGC2**$^{+\bullet}$, **dGC3**$^{+\bullet}$, and **dGC5**$^{+\bullet}$, see the respective Figure S14a−c in the Supporting Information. Conformational collapse in **dGC1**$^{+\bullet}$ resulting in nucleobase stacking formed isomer **dGC6**$^{+\bullet}$ that was a cytosine radical comparably stable as **dGC1**$^{+\bullet}$. The absorption spectrum of **dGC6**$^{+\bullet}$ (Figure S14d, Supporting Information) was similar to the spectra of **dGC1**$^{+\bullet}$ and **dGC4**$^{+\bullet}$ with the exception of weaker bands in the 230−250 nm region. The lowest-energy $(dGC + 2H)^{+\bullet}$ isomer was obtained by a hydrogen atom transfer from the cytosine N-3 position to C-8 at guanine, yielding the 7,8-dihydroguanine cation radical **dGC7**$^{+\bullet}$ (Scheme 4). However, the calculated absorption spectrum of **dGC7**$^{+\bullet}$ (Figure S14e) showed bands at 336 and 376 nm that did not have equivalents in the action spectrum of $(dGC+ 2H)^{+\bullet}$. The spectroscopic data led us to conclude that the $(dGC + 2H)^{+\bullet}$ formed by ETD were cytosine radicals. A more specific assignment of the cation-radical conformation and the protomeric form of the charged guanine ring relied on the energy data alone. The precursor

Table 3. Relative Energies of $(dGC + 2H)^{+\bullet}$ Ions

	relative energy[a,b]				
ion	B3LYP[c]	ωB97X-D[c]	M06-2X[c]	PMP2[c]	ROMP2[c]
dGC1$^{+\bullet}$	0 (0)[d]	0 (0)	0 (0)	0 (0)	0 (0)
dGC2$^{+\bullet}$	22 (21)	6 (5)	7 (6)	16 (15)	17 (16)
dGC3$^{+\bullet}$	8 (6)	9 (7)	17 (15)	16 (14)	17 (15)
dGC4$^{+\bullet}$	13 (17)	12 (15)	13 (17)	11 (14)	12 (15)
dGC5$^{+\bullet}$	−5 (10)	2 (17)	14 (29)	−30 (−15)	−37 (−22)
dGC6$^{+\bullet}$	26 (39)	−1 (12)	11 (24)	−7 (6)	−14 (−1)
dGC7$^{+\bullet}$	−15 (−4)	−34 (−23)	−60 (−50)	−29 (−18)	−27 (−16)
dGC-TS	94	82	95	69	71

[a]In kJ mol^{-1}. [b]Including B3LYP/6-31+G(d,p) zero-point vibrational energy corrections. [c]Single-point calculations with the 6-311++G(2d,p) basis set. [d]Values in parentheses are relative free energies at 310 K.

DOI: 10.1021/acs.jpcb.8b07925
J. Phys. Chem. B 2018, 122, 9665−9680

Scheme 5. Isomerization of $(GC + 2H)^{+\bullet}$ Cation Radicals[a]

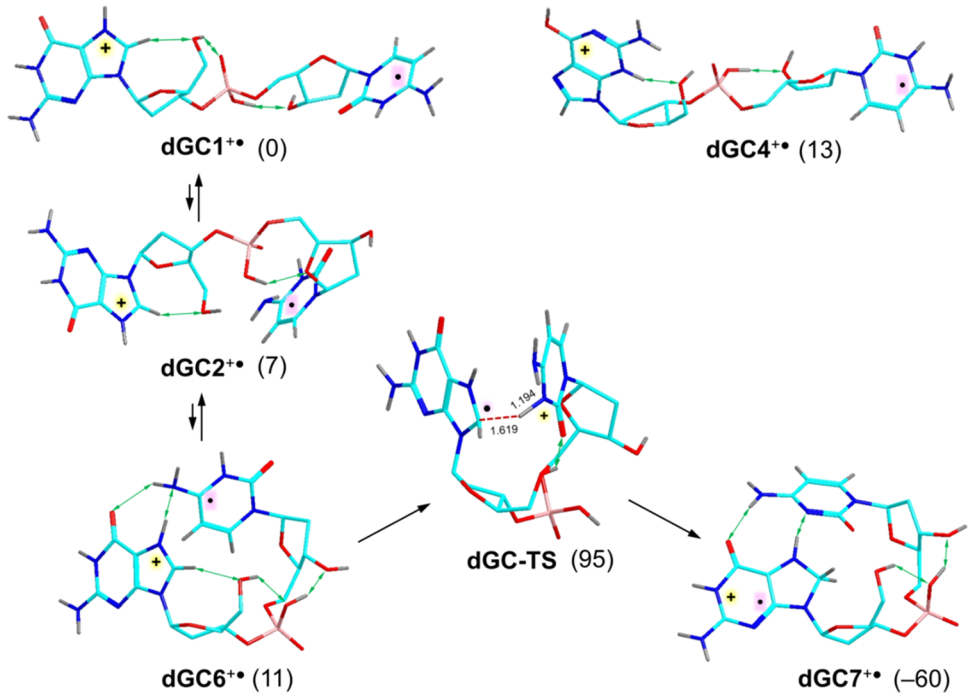

[a]Relative energies (kJ mol^{-1}) are from M06-2X/6-311++G(2d,p) calculations including zero-point vibrational energies and refer to 0 K. For energies from the other calculations, see Table 3.

dications preferred guanine protonation at N-7, disfavoring the formation of the protomeric isomers $GC4^{2+}$–$GC6^{2+}$ that would have formed cation radical $dGC4^{+\bullet}$ upon electron transfer. Hence, based on both relative energies and action spectra, ion $dGC1^{+\bullet}$ and its conformers appear to be the best match for the $(GC + 2H)^{+\bullet}$ cation radicals formed by electron transfer.

DISCUSSION

The above-described structural analysis raised several points regarding the formation and properties of the hydrogen-rich dinucleotide cation radicals. The site of electron attachment to the dications was found to depend on both the nucleobase nature and position. Electron attachment to the cytosine–guanine combinations $(CG + 2H)^{2+}$ and $(GC + 2H)^{2+}$ favored the formation of cytosine radicals, e.g., $dCG1^{+\bullet}$ and $dGC1^{+\bullet}$. Low-energy guanine-centered radicals such as $dCG6^{+\bullet}$ and $dGC7^{+\bullet}$ were formed as secondary products of hydrogen atom or proton migration targeting the guanine C-8 position. The preferential electron attachment to protonated cytosine can be related to its higher adiabatic recombination energy, RE_{adiab} = 5.17 eV for the N-3–H tautomer,[76] compared to that of the N-7, N-9–H tautomer of protonated guanine, RE_{adiab} = 4.46 eV. Both these RE_{adiab} values were calculated on the same level of ab initio theory (CCSD(T)/6-311++G(3df,2p); Table S4, Supporting Information). In the case of nearly identical nucleobases such as the N-7-protonated guanines in $(GG + 2H)^{2+}$, electron attachment favored the 5′-ring ($dGG1a^{+\bullet}$). This outcome was probably caused by the stabilization of the 3′-cation by a hydrogen bond between the guanine H-8 and phosphodiester O═P oxygen, which was facilitated by their syn arrangement on the 3′-deoxyribose ring. We note that a similar dipolar interaction has been reported by Rodgers et al. for singly protonated guanosine and 2′-deoxyguanosine cations.[74] In contrast, the antiarrangement of the 5′-guanine cation and the P═O bond prevents the formation of a C-8–H···O═P hydrogen bond.

Another feature distinguishing the guanine and cytosine cation radicals was their different tendencies to undergo ring stacking and isomerize by proton transfer. With $dGG1^{+\bullet}$ that was initially formed by one-electron reduction of the dication, stacking to $dGG1b^{+\bullet}$ was 98 kJ mol^{-1} exothermic, which was greater than the stacking energy calculated by Hobza and Sponer for a neutral guanine–guanine pair (54 kJ mol^{-1}).[79] The nucleobase stacking in $dGG1b^{+\bullet}$ was constrained by the deoxyribose and phosphate backbone to reach a 60° angle between the rings. The large stabilization of $dGG1b^{+\bullet}$ can be ascribed to the formation of multiple hydrogen bonds involving N-7–H and O-6 of the 5′-guanine and N-1–H, NH_2, and O-6 of the 3′-guanine (Scheme 2). Interestingly, the 5′-hydroxyl developed a H-bond to the C-8 radical, which was analogous to H-bonds in alkyl radicals.[80] The angle between the rings and guanine hydrogen bonding was largely preserved in **dGG-TS**, involving N-7 proton transfer from the 3′-guanine ion to the C-8 position on the 5′-guanine radical, which was catalytically relayed by the 5′-hydroxyl, resulting in an extremely low energy transition state (Scheme 2). Ring stacking was further enhanced in 3′-radicals $dGG1d^{+\bullet}$ and $dGG1e^{+\bullet}$, in which the guanine rings were positioned at a 30° angle. However, another low-energy 5′-radical, $dGG1f^{+\bullet}$, had rings close to 90° and the stabilizing inter-ring interaction was chiefly due to a strong hydrogen bond between the 5′-guanine O-6 and 3′-guanine N-7–H at 1.66 Å (Scheme 2).

Stacking interactions between the nucleobases were absent in $dCG^{+\bullet}$ and $dGC^{+\bullet}$. Both the 5′-cytosine radical $dCG1^{+\bullet}$ and its isomerized 3′-guanine radical product $dCG6^{+\bullet}$ showed a nearly perpendicular arrangement of the nucleobase rings (Figure 6b,c). The attractive inter-ring interaction in $dCG1^{+\bullet}$

DOI: 10.1021/acs.jpcb.8b07925
J. Phys. Chem. B 2018, 122, 9665–9680

Scheme 6. Proton Transfer in (G + H)• and (C + H)•[a]

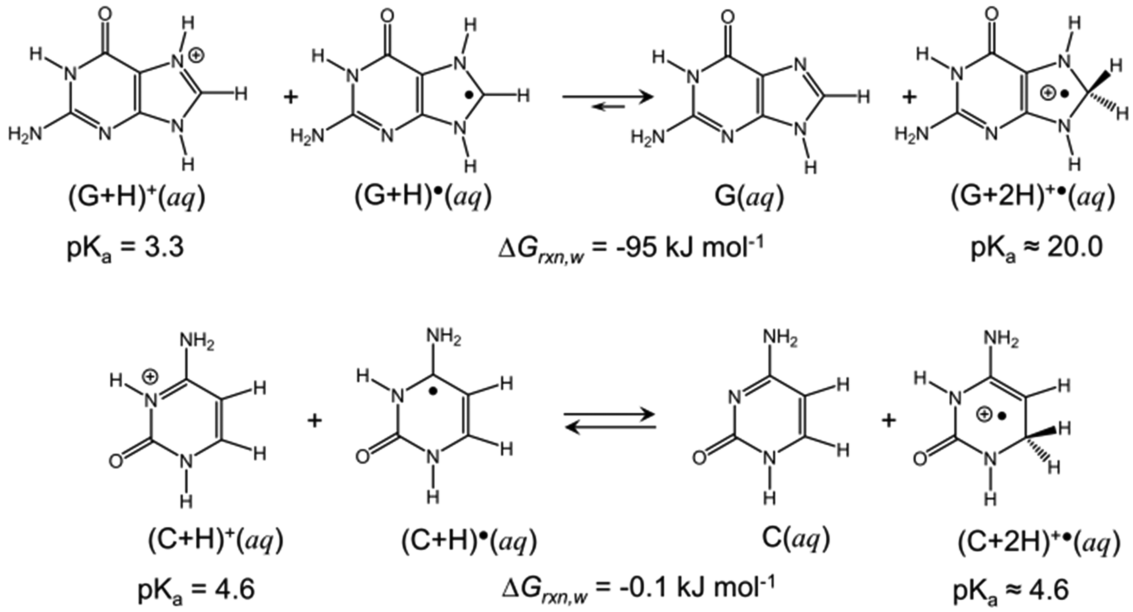

[a]Average free energies are from calculations in Table S4.

was chiefly due to a single strong H-bond (at d(O···H) = 1.50 Å) between O-2 of the 5′-cytosine radical and N-7−H of the guanine ion. This H-bonding interaction (at d(O···H) = 1.61 Å) was preserved in **dCG6**$^{+\bullet}$. Regarding the isomerization of **dCG1**$^{+\bullet}$, spin density analysis of the reactant (**dCG1**$^{+\bullet}$) and the transition state (**dCG-TS1**) indicated a proton-coupled electron-transfer process (Scheme 4). According to the natural population analysis of **dCG1**$^{+\bullet}$ and **dCG-TS1**, the unpaired electron density that was initially localized in the cytosine ring in **dCG1**$^{+\bullet}$ moved to guanine in **dCG-TS1**, which was followed by a transfer of the cytosine N-3 proton. The transition-state energy for **dCG-TS1** (106 kJ mol^{-1}) was notably higher than that for **dGG-TS** (9 kJ mol^{-1}, Scheme 2). We identified another isomerization pathway consisting of an endothermic migration of the guanine N-7−H to the cytosine 2-O (**dCG4**$^{+\bullet}$), followed by reverse proton transfer to guanine C-8 (**dCG-TS2**, Scheme 4). This can be viewed as a cytosine-radical-catalyzed migration of guanine N-7−H to the stabilized C-8 position. This pathway may avoid a direct 1,2-H migration of guanine N-7−H, which was presumed to require a much higher energy in the pertinent transition state. However, the formation of **dCG4**$^{+\bullet}$ was unlikely to proceed without internal catalysis because the transition state for a direct **dCG1**$^{+\bullet}$ → **dCG4**$^{+\bullet}$ isomerization via a 1,3-hydrogen shift was calculated to require a high-energy transition state (**dCG-TS3**, Scheme 4).

Hydrogen bonding between the nucleobases was not realized in (dGC + 2H)$^{+\bullet}$ isomers **dGC1**$^{+\bullet}$ and **dGC4**$^{+\bullet}$, which were identified as the major products of one-electron reduction. Conformational folding in **dGC1**$^{+\bullet}$, resulting in nucleobase cation-radical interactions, did not produce a lower-energy conformer. The folded structures **dGC5**$^{+\bullet}$ and **dGC6**$^{+\bullet}$ were disfavored against **dGC1**$^{+\bullet}$ by entropy and were not likely to dominate under thermal equilibrium conditions. A large negative change of entropy (−34 J mol^{-1} K^{-1}) was also associated with attaining the transition state for proton migration, **dGC1**$^{+\bullet}$ → **dGC-TS**, which may explain slow isomerization to **dGC7**$^{+\bullet}$ and retention of **dGC1**$^{+\bullet}$ conformers after ETD.

The facile hydrogen transfer between the guanine nucleobases in gas-phase (dGG+ 2H)$^{+\bullet}$ raised the question of proton or hydrogen atom migration in DNA cation radicals in solution, which was relevant to chemical changes in DNA following ionization. Hydrogen-rich DNA radicals are formed by protonation of anion radicals following fast capture of a low-energy electron.[40] We addressed this topic with model lowest-energy guanine and cytosine radicals (Scheme 5, 6 and Table S4, Supporting Information) and their respective 9-methylguanine and 1-methylcytosine homologues (Table S5) to account for the effect of the pertinent deoxyribose substituents. According to our DFT calculations, proton transfer from (G + H)$^+$(aq) to (G + H)$^\bullet$(aq) was highly exothermic, $\Delta G_{rxn,w}$ = −95 kJ mol^{-1} (average value from Table S4, Supporting Information), producing G(aq) and the hydrogen-rich cation radical (G + 2H)$^{+\bullet}$(aq). Combining $\Delta G_{rxn,w}$ with the pK_a of guanine (pK_a = 3.3),[81,82] one obtains pK_a for (G + 2H)$^{+\bullet}$ ranging from 19.8 to 20.2. This indicates that (G + H)$^\bullet$ should be a superbase in water and react rapidly with solvent, forming (G + 2H)$^{+\bullet}$ over a range of pH values. In contrast, DFT calculations of the hydrogen-rich cytosine cation radical, (C + 2H)$^{+\bullet}$(aq), indicated facile deprotonation, yielding an average pK_a = 4.6 when adjusted to the pK_a of guanine (Table S4, Supporting Information). Thus, protonation of (C + H)$^\bullet$ by water can be expected to be sensitive to the solution pH and cytosine environment in DNA (Scheme 6).[83] The effect of the deoxyribose substituent in 2′-deoxyguanosine and 2′-deoxycytidine on pK_a was modeled by the pertinent methyl-substituted nucleobases. Averaged computational data from Table S5 (Supporting Information) indicated a slight increase of basicity, as expressed by the pK_a's of 20.8 and 5.4 for 9-methylguanosine and 1-methylcytosine, respectively. We note that various aspects of proton transfer involving guanine−cytosine base pairs in the cation-radical[15,16,19] or anion-radical forms[22,23] have been studied and discussed.[20,21] However, to the best of our knowledge, pK_a values of neutral nucleobase

DOI: 10.1021/acs.jpcb.8b07925
J. Phys. Chem. B 2018, 122, 9665−9680

radicals have not been determined, and thus our reported values provide insight into the protonation energetics of these transient species.

CONCLUSIONS

The experimental and computational data reported here allowed us to arrive at the following conclusions. DNA dinucleotide cation radicals of a new hydrogen-rich type were prepared in high yield and purity by electron-transfer dissociation of dication−crown−ether complexes. Crown−ether complexation in the dications depended on the nucleobase and its 3′ or 5′ position and stabilized dinucleotide protomers with N-7-protonated guanine and N-3-protonated cytosine.

Photodissociation action spectroscopy provided spectra for $(dGG + 2H)^{+\bullet}$, $(dCG + 2H)^{+\bullet}$, and $(dGC + 2H)^{+\bullet}$ that were interpreted by TD-DFT calculations and assigned to nucleobase radical structural types formed directly by electron attachment or after rearrangement. Radical−cation nucleobase interactions in $(dGG + 2H)^{+\bullet}$ resulted in exothermic conformational collapse that commenced by nucleobase stacking and was followed by hydrogen migration between the nucleobases, forming stable guanine-8,8-H_2 radicals. Contrasting this, conformational folding in $(dCG + 2H)^{+\bullet}$ and $(dGC + 2H)^{+\bullet}$ was slightly endoergic and did not involve nucleobase stacking. Hydrogen transfer from cytosine to guanine, albeit exothermic, was kinetically hampered.

ASSOCIATED CONTENT

Supporting Information

The Supporting Information is available free of charge on the ACS Publications website at DOI: 10.1021/acs.jpcb.8b07925.

> Relative energies of dications; ETD and ETD-UVPD-MS^3 spectra; UV photodissociation action spectra of cations; ωB97X-D/6-31+G(d,p)-optimized structures of dication−crown−ether complexes; M06-2X/6-31+G-(d,p) TD-DFT-calculated UV−vis absorption spectra of cation radicals; orbital diagrams; and RRKM-calculated rate constants and mole fractions (PDF)

AUTHOR INFORMATION

Corresponding Author

*E-mail: turecek@chem.washington.edu.

ORCID

František Tureček: 0000-0001-7321-7858

Author Contributions

†Y.L. and J.A.K. contributed equally to this work and both should be considered first authors.

Notes

The authors declare no competing financial interest.

ACKNOWLEDGMENTS

Financial support from the Chemistry Division of the National Science Foundation (Grants CHE-1661815 for experiments and CHE-1624430 for calculations) is gratefully acknowledged. F.T. acknowledges the Klaus and Mary Ann Saegebarth Endowment for general support.

REFERENCES

(1) Khanna, K. K.; Jackson, S. P. DNA Double-Strand Breaks: Signalling, Repair and the Cancer Connection. *Nat. Genet.* **2001**, *27*, 247−254.

(2) Wagenknecht, H.-A., Ed. *Charge Transfer in DNA*; Wiley-VCH: Weinheim, Germany, 2005; pp 1−23.

(3) Schuster, G. B. Long-Range Charge Transfer in DNA: Transient Structural Distortions Control the Distance Dependence. *Acc. Chem. Res.* **2000**, *33*, 253−260.

(4) O'Neill, M. A.; Barton, J. K. Sequence-Dependent DNA Dynamics: The Regulator of DNA-Mediated Charge Transport. In *Charge Transfer in DNA*; Wagenknecht, H.-A., Ed.; Wiley-VCH: Weinheim, Germany, 2005; pp 27−31.

(5) Giese, B. Long-Distance Charge Transport in DNA: The Hopping Mechanism. *Acc. Chem. Res.* **2000**, *33*, 631−636.

(6) Giese, B.; Amaudrut, J.; Kohler, A. K.; Spormann, M.; Wessely, S. Direct Observation of Hole Transfer Through DNA by Hopping Between Adenine Bases and by Tunnelling. *Nature* **2001**, *412*, 318−320.

(7) Douki, T.; Ravanat, J.-L.; Angelov, D.; Wagner, J. R.; Cadet, J. Effects of Duplex Stability on Charge-Transfer Efficiency within DNA. *Top. Curr. Chem.* **2004**, *236*, 1−25.

(8) Joy, A.; Ghosh, A. K.; Schuster, G. B. One-Electron Oxidation of DNA Oligomers That Lack Guanine: Reaction and Strand Cleavage at Remote Thymines by Long-Distance Radical Cation Hopping. *J. Am. Chem. Soc.* **2006**, *128*, 5346−5347.

(9) Ghosh, A.; Joy, A.; Schuster, G. B.; Douki, T.; Cadet, J. Selective One-Electron Oxidation of Duplex DNA Oligomers: Reaction at Thymines. *Org. Biomol. Chem.* **2008**, *6*, 916−928.

(10) Joseph, J.; Schuster, G. B. Oxidatively Damaged Nucleobases in Duplex DNA Oligomers: Reaction at Thymine-Thymine Mispairs. *J. Am. Chem. Soc.* **2009**, *131*, 13904−13905.

(11) Kanvah, S.; Schuster, G. B. One-Electron Oxidation of DNA: Thymine versus Guanine Reactivity. *Org. Biomol. Chem.* **2010**, *8*, 1340−1343.

(12) Kanvah, S.; Joseph, J.; Schuster, G. B.; Barnett, R. N.; Cleveland, C. L.; Landman, U. Oxidation of DNA: Damage to Nucleobases. *Acc. Chem. Res.* **2010**, *43*, 280−287.

(13) Kravec, S. M.; Kinz-Thompson, C. D.; Conwell, E. M. Localization of a Hole on an Adenine-Thymine Radical Cation in BForm DNA in Water. *J. Phys. Chem. B* **2011**, *115*, 6166−6171.

(14) Barnett, R. N.; Joseph, J.; Landman, U.; Schuster, G. B. Oxidative Thymine Mutation in DNA: Water-Wire-Mediated Proton-Coupled Electron Transfer. *J. Am. Chem. Soc.* **2013**, *135*, 3904−3914.

(15) Cauët, E.; Lievin, J. Radical Cations of the Nucleic Bases and Radiation Damage to DNA: Ab Initio Study. *Adv. Quantum Chem.* **2007**, *52*, 121−147.

(16) Rodriguez-Santiago, L.; Noguera, M.; Bertan, J.; Sodupe, M. Hydrogen Bonding and Proton Transfer in Ionized DNA Base Pairs, Amino Acids and Peptides. In *Quantum Biochemistry*; Matt, C. F., Ed.; Wiley-VCH: Weinheim, Germany, 2010; pp 219−242.

(17) Li, X.; Cai, Z.; Sevilla, M. D. Investigation of Proton Transfer within DNA Base Pair Anion and Cation Radicals by Density Functional Theory (DFT). *J. Phys. Chem. B* **2001**, *105*, 10115−10123.

(18) Wang, M.; Zhao, J.; Bu, Y. Theoretical Exploration of Structures and Electronic Properties of Double-Electron Oxidized Guanine-Cytosine Base Pairs with Intriguing Radical-Radical Interactions. *Phys. Chem. Chem. Phys.* **2013**, *15*, 18453−18463.

(19) Choi, J.; Yang, C.; Fujitsuka, M.; Tojo, S.; Ihee, H.; Majima, T. Proton Transfer of Guanine Radical Cations Studied by Time-Resolved Resonance Raman Spectroscopy Combined with Pulse Radiolysis. *J. Phys. Chem. Lett.* **2015**, *6*, 5045−5050.

(20) Sevilla, M. D.; Kumar, A.; Adhikary, A. Comment on "Proton Transfer of Guanine Radical Cations Studied by Time-Resolved Resonance Raman Spectroscopy Combined with Pulse Radiolysis". *J. Phys. Chem. B* **2016**, *120*, 2984−2986.

(21) Choi, J.; Yang, C.; Fujitsuka, M.; Tojo, S.; Ihee, H.; Majima, T. Reply to Comment on "Proton Transfer of Guanine Radical Cations

Studied by Time-Resolved Resonance Raman Spectroscopy Combined with Pulse Radiolysis". *J. Phys. Chem. B* **2016**, *120*, 2987−2989.
(22) Lin, Y.; Wang, H.; Gao, S.; Li, R.; Schaefer, H. F. Hydrogen-Bonded Double-Proton Transfer in Five Guanine-Cytosine Base Pairs after Hydrogen Atom Addition. *J. Phys. Chem. B* **2012**, *116*, 8908−8915.
(23) Hsu, S. C. N.; Wang, T.-P.; Kao, C.-L.; Chen, H.-F.; Yang, P.-Y.; Chen, H.-Y. Theoretical Study of the Protonation of the One-Electron-Reduced Guanine-Cytosine Base Pair by Water. *J. Phys. Chem. B* **2013**, *117*, 2096−2105.
(24) Feketeová, L.; Chan, B.; Khairallah, G. N.; Steinmetz, V.; Maitre, P.; Radom, L.; O'Hair, R. A. J. Watson-Crick Base Pair Radical Cation as a Model for Oxidative Damage in DNA. *J. Phys. Chem. Lett.* **2017**, *8*, 3159−3165.
(25) Wolken, J. K.; Syrstad, E. A.; Vivekananda, S.; Turecek, F. Uracil Radicals in the Gas Phase. Specific Generation and Energetics. *J. Am. Chem. Soc.* **2001**, *123*, 5804−5805.
(26) Chen, X.; Syrstad, E. A.; Nguyen, M. T.; Gerbaux, P.; Turecek, F. Distonic Isomers and Tautomers of the Adenine Cation Radical in the Gas Phase and Aqueous Solution. *J. Phys. Chem. A* **2004**, *108*, 9283−9293.
(27) Yao, C.; Cuadrado-Peinado, M.; Polasek, M.; Turecek, F. Specific Generation of 1-Methylcytosine Radicals in the Gas-Phase. *Angew. Chem., Int. Ed.* **2005**, *44*, 6708−6711.
(28) Lam, A. K.; Abrahams, B. F.; Grannas, M. J.; McFadyen, W. D.; O'Hair, R. A. J. Tuning the Gas Phase Redox Properties of Copper(II) Ternary Complexes of Terpyridines to Control the Formation of Nucleobase Radical Cations. *Dalton Trans.* **2006**, 5051−5061.
(29) Wee, S.; O'Hair, R. A. J.; McFadyen, W. D. Can Radical Cations of the Constituents of Nucleic Acids Be Formed in the Gas Phase Using Ternary Transition Metal Complexes? *Rapid Commun. Mass Spectrom.* **2005**, *19*, 1797−1805.
(30) Feketeová, L.; Khairallah, G. N.; Chan, B.; Steinmetz, V.; Maître, P.; Radom, L.; O'Hair, R. A. J. Gas-Phase Infrared Spectrum and Acidity of the Radical Cation of 9-Methylguanine. *Chem. Commun.* **2013**, *49*, 7343−7345.
(31) Lesslie, M.; Lawler, J. T.; Dang, A.; Korn, J. A.; Bím, D.; Steinmetz, V.; Maitre, P.; Turecek, F.; Ryzhov, V. Cytosine Radical Cation: A Gas- Phase Study Combining IRMPD Spectroscopy, UV-PD Spectroscopy, Ion−Molecule Reactions, and Theoretical Calculations. *ChemPhysChem* **2017**, *18*, 1293−1301.
(32) Dang, A.; Nguyen, H. T. H.; Ruiz, H.; Piacentino, E.; Ryzhov, V.; Tureček, F. Experimental Evidence for Non-Canonical Thymine Cation Radicals in the Gas Phase. *J. Phys. Chem. B* **2018**, *122*, 86−97.
(33) Tureček, F. Transient Intermediates of Chemical Reactions by Neutralization-Reionization Mass Spectrometry. In *Modern Mass Spectrometry*; Schalley, C. A., Ed.; Topics in Current Chemistry; Springer: Berlin, 2003; Vol. *225*, pp 77−129.
(34) Korn, J. A.; Urban, J.; Dang, A.; Nguyen, H. T. H.; Turecek, F. UV-Vis Action Spectroscopy Reveals a Conformational Collapse in Hydrogen-Rich Dinucleotide Cation Radicals. *J. Phys. Chem. Lett.* **2017**, *8*, 4100−4107.
(35) McLuckey, S. A.; Huang, T.-Y. Ion/Ion Reactions: New Chemistry for Analytical MS. *Anal. Chem.* **2009**, *81*, 8669−8676.
(36) Syka, J. E. P.; Coon, J. J.; Schroeder, M. J.; Shabanowitz, J.; Hunt, D. F. Peptide and Protein Sequence Analysis by Electron Transfer Dissociation Mass Spectrometry. *Proc. Natl. Acad. Sci. U.S.A.* **2004**, *101*, 9528−9533.
(37) Zubarev, R. A. Reactions of polypeptide ions with electrons in the gas phase. *Mass Spectrom. Rev.* **2003**, *22*, 57−77.
(38) Tureček, F.; Julian, R. R. Peptide Radicals and Cation-Radicals in the Gas Phase. *Chem. Rev.* **2013**, *113*, 6691−6733.
(39) Westphal, K.; Wiczk, J.; Miloch, J.; Kciuk, G.; Bobrowski, K.; Rak, J. Irreversible Electron Attachment - A Key to DNA Damage by Solvated Electrons in Aqueous Solution. *Org. Biomol. Chem.* **2015**, *13*, 10362−10369.
(40) Steenken, S. Purine Bases, Nucleosides, and Nucleotides: Aqueous Solution Redox Chemistry and Transformation Reactions of Their Radical Cations and e- and OH Adducts. *Chem. Rev.* **1989**, *89*, 503−520.
(41) Antoine, R.; Dugourd, P. UV−Visible Activation of Biomolecular Ions. In *Laser Photodissociation and Spectroscopy of Mass-separated Biomolecular Ions*; Polfer, N., Dugourd, P., Eds.; Lecture Notes in Chemistry; Springer: Cham, 2013; Vol. *83*, pp 93−116.
(42) Polfer, N. C.; Dugourd, P., Eds. *Laser Photodissociation and Spectroscopy of Mass Separated Biomolecular Ions*; Lecture Notes in Chemistry; Springer: Cham, 2013; Vol. *83*, pp 13−20.
(43) Furche, F.; Ahlrichs, A. Adiabatic Time-Dependent Density Functional Methods for Excited State Properties. *J. Chem. Phys.* **2002**, *117*, 7433−7447.
(44) Comeau, D. C.; Bartlett, R. J. The Equation-of-Motion Coupled- Cluster Method. Applications to Open- and Closed-Shell Reference States. *Chem. Phys. Lett.* **1993**, *207*, 414−423.
(45) Shaffer, C. J.; Pepin, R.; Tureček, F. Combining UV Photodissociation Action Spectroscopy with Electron Transfer Dissociation for Structure Analysis of Gas-Phase Peptide Cation-Radicals. *J. Mass Spectrom.* **2015**, *50*, 1438−1442.
(46) Nguyen, H. T. H.; Shaffer, C. J.; Pepin, R.; Tureček, F. UV Action Spectroscopy of Gas-Phase Peptide Radicals. *J. Phys. Chem. Lett.* **2015**, *6*, 4722−4727.
(47) Viglino, E.; Shaffer, C. J.; Tureček, F. UV−Vis Action Spectroscopy and Structures of Tyrosine Peptide Cation Radicals in the Gas Phase. *Angew. Chem., Int. Ed.* **2016**, *55*, 7469−7473.
(48) Stewart, J. J. P. Optimization of Parameters for Semi-Empirical Methods. V. Modification of NDDO Approximations and Application to 70 Elements. *J. Mol. Model.* **2007**, *13*, 1173−1213.
(49) Řezáč, J.; Fanfrlík, J.; Salahub, D.; Hobza, P. Semi-Empirical Quantum Chemical PM6Method Augmented by Dispersion and H Bonding Correction Terms Reliably Describes Various Types of Noncovalent Complexes. *J. Chem. Theory Comput.* **2009**, *5*, 1749−1760.
(50) Stewart, J. J. P. MOPAC 16. *Stewart Computational Chemistry*; Colorado Springs: CO, 2016.
(51) Řezáč, J. Cuby: An Integrative Framework for Computational Chemistry. *J. Comput. Chem.* **2016**, *37*, 1230−1237.
(52) Nguyen, H. T. H.; Andrikopoulos, P. C.; Bím, D.; Rulíšek, L.; Dang, A.; Tureček, F. Radical Reactions Affecting Polar Groups in Threonine Peptide Ions. *J. Phys. Chem. B* **2017**, *121*, 6557−6569.
(53) Berendsen, H. J.; Postma, J. V.; van Gunsteren, W. F.; DiNola, A. R. H. J.; Haak, J. R. Molecular Dynamics with Coupling to an External Bath. *J. Chem. Phys.* **1984**, *81*, 3684−3690.
(54) Becke, A. D. Density-Functional Exchange-Energy Approximation with Correct Asymptotic Behavior. *Phys. Rev. A* **1988**, *38*, 3098−3100.
(55) Chai, J. D.; Head-Gordon, M. Long-Range Corrected Hybrid Density Functionals with Damped Atom-Atom Dispersion Corrections. *Phys. Chem. Chem. Phys.* **2008**, *10*, 6615−6620.
(56) Tomasi, J.; Mennucci, B.; Cammi, R. Quantum Mechanical Continuum Solvation Models. *Chem. Rev.* **2005**, *105*, 2999−3093.
(57) Zhao, Y.; Truhlar, D. G. The M06 Suite of Density Functionals for Main Group Thermochemistry, Thermochemical Kinetics, Noncovalent Interactions, Excited States, and Transition Elements: Two New Functionals and Systematic Testing of Four M06-Class Functionals and 12 Other Functionals. *Theor. Chem. Acc.* **2008**, *120*, 215−241.
(58) Møller, C.; Plesset, M. S. A Note on an Approximation Treatment for Many-Electron Systems. *Phys. Rev.* **1934**, *46*, 618−622.
(59) Schlegel, H. B. Potential Energy Curves Using Unrestricted Moller-Plesset Perturbation Theory with Spin Annihilation. *J. Chem. Phys.* **1986**, *84*, 4530.
(60) Mayer, I. Spin-Projected UHF Method. IV. Comparison of Potential Curves Given by Different One-Electron Methods. *Adv. Quantum Chem.* **1978**, *14*, 29−38.
(61) Chan, B.; Radom, L. Assessment of Theoretical Procedures for Hydrogen-Atom Abstraction by Chblorine and Relate Reactions. *Theor. Chem. Acc.* **2011**, *130*, 251−260.

DOI: 10.1021/acs.jpcb.8b07925
J. Phys. Chem. B 2018, 122, 9665−9680

(62) Reed, A. E.; Weinstock, R. B.; Weinhold, F. Natural Population Analysis. *J. Chem. Phys.* **1985**, *83*, 735−746.
(63) Frisch, M. J.; Trucks, G. W.; Schlegel, H. B.; Scuseria, G. E.; Robb, M. A.; Cheeseman, J. R.; Scalmani, G.; Barone, V.; Petersson, G. A.; Nakatsuji, H. et al. *Gaussian 16*, revision A01; Gaussian, Inc.: Wallingford, CT, 2016.
(64) Gilbert, R. G.; Smith, S. C. *Theory of Unimolecular and Recombination Reactions*; Blackwell Scientific Publications: Oxford, 1990; pp 52−132.
(65) Zhu, L.; Hase, W. L. *Quantum Chemistry Program Exchange*, Program No. QCPE 644; Indiana University: Bloomington, 1994.
(66) Frank, A. J.; Sadílek, M.; Ferrier, J. G.; Turecek, F. Sulfur Oxoacids and Radicals in the Gas Phase. A Variable-Time Neutralization-Photoexcitation- Reionization Mass Spectrometric and Ab initio/RRKM Study. *J. Am. Chem. Soc.* **1997**, *119*, 12343−12353.
(67) Hari, Y.; Leumann, C. J.; Schurch, S. What Hinders Electron Transfer Dissociation (ETD) of DNA Cations? *J. Am. Soc. Mass Spectrom.* **2017**, *28*, 2677−2685.
(68) Viglino, E.; Lai, C. K.; Mu, X.; Chu, I. K.; Tureček, F. Ground and Excited-Electronic-State Dissociations of Hydrogen-Rich and Hydrogen-Deficient Tyrosine Peptide Cation Radicals. *J. Am. Soc. Mass Spectrom.* **2016**, *27*, 1454−1467.
(69) Murray, K. DNA Sequencing by Mass Spectrometry. *J. Mass Spectrom.* **1996**, *31*, 1203−1215.
(70) Petroselli, G.; Dantola, M. L.; Cabrerizo, F. M.; Capparelli, A. L.; Lorente, C.; Oliveros, E.; Thomas, A. H. Oxidation of 2′-Deoxyguanosine 5′-Monophosphate Photoinduced by Pterin: Type I versus Type II Mechanism. *J. Am. Chem. Soc.* **2008**, *130*, 3001−3011.
(71) Zhang, Y.; Improta, R.; Kohler, B. Mode-Specific Vibrational Relaxation of Photoexcited Guanosine 5′-Monophosphate and Its Acid Form: A Femtosecond Broadband Mid-IR Transient Absorption and Theoretical Study. *Phys. Chem. Chem. Phys.* **2014**, *16*, 1487−1499.
(72) Colominas, C.; Luque, F. J.; Orozco, M. Tautomerism and Protonation of Guanine and Cytosine. Implications in the Formation of Hydrogen-Bonded Complexes. *J. Am. Chem. Soc.* **1996**, *118*, 6811−6821.
(73) Halder, A.; Bhattacharya, S.; Datta, A.; Bhattacharya, D.; Mitra, A. The Role of N7 Protonation of Guanine in Determining the Structure, Stability and Function of RNA Base Pairs. *Phys. Chem. Chem. Phys.* **2015**, *17*, 26249−26263.
(74) Wu, R. R.; Yang, B.; Berden, G.; Oomens, J.; Rodgers, M. T. Gas-Phase Conformations and Energetics of Protonated 2-Deoxyguanosine and Guanosine: IRMPD Action Spectroscopy and Theoretical Studies. *J. Phys. Chem. B* **2014**, *118*, 14774−14784.
(75) Barbatti, M.; Ruckenbauer, M.; Plasser, F.; Pittner, J.; Granucci, G.; Persico, M.; Lischka, H. Newton-X: A Surface-Hopping Program for Nonadiabatic Molecular Dynamics. *Wiley Interdiscip. Rev.: Comput. Mol. Sci.* **2014**, *4*, 26−33.
(76) Yao, C.; Tureček, F.; Polce, M. J.; Wesdemiotis, C. Proton and Hydrogen Atom Adducts to Cytosine. An Experimental and Computational Study. *Int. J. Mass Spectrom.* **2007**, *265*, 106−123.
(77) Yao, C.; Cuadrado-Peinado, M.; Polášek, M.; Tureček, F. Gas-Phase Tautomers of Protonated 1-Methylcytosine. Preparation, Energetics and Dissociation Mechanisms. *J. Mass Spectrom.* **2005**, *40*, 1417−1428.
(78) Michl, J. Electronic Spectrum of Fluoranthene. *J. Mol Spectrosc.* **1969**, *30*, 66−76.
(79) Hobza, P.; Sponer, J. Toward True DNA Base-Stacking Energies: MP2, CCSD(T), and Complete Basis Set Calculations. *J. Am. Chem. Soc.* **2002**, *124*, 11802−11808.
(80) Hammerum, S. Alkyl Radicals as Hydrogen Bond Acceptors: Computational Evidence. *J. Am. Chem. Soc.* **2009**, *131*, 8627−8635.
(81) Fasman, G. D. *CRC Handbook of Biochemistry and Molecular Biology. Nucleic Acids*, 3rd ed.; CRC Press: Cleveland, OH, 1975; Vol. *1*.
(82) Dawson, R. M. C.; Elliott, D. C.; Elliott, W. H.; Jones, K. M. *Data for Biochemical Research*, 3rd ed.; Oxford University Press: Oxford, 1986.
(83) Verdolino, V.; Cammi, R.; Munk, B. H.; Schlegel, H. B. Calculation of pK_a Values of Nucleobases and the Guanine Oxidation Products Guanidinohydantoin and Spiro-iminodihydantoin Using Density Functional Theory and a Polarizable Continuum Model. *J. Phys. Chem. B* **2008**, *112*, 16860−16863.

DOI: 10.1021/acs.jpcb.8b07925
J. Phys. Chem. B 2018, 122, 9665−9680